(4)

Applied Research Laboratory

Technical Report

FABRICATION OF UNIDIRECTIONAL FIBER
REINFORCED 6061 ALUMINUM ALLOY
USING HIGH PRESSURE SQUEEZE CASTING

by

Robert J. Sample
Ram B. Bhagat

PENNSTATE

4

The Pennsylvania State University
APPLIED RESEARCH LABORATORY
P.O. Box 30
State College, PA 16804

FABRICATION OF UNIDIRECTIONAL FIBER REINFORCED 6061 ALUMINUM ALLOY USING HIGH PRESSURE SQUEEZE CASTING

by

Robert J. Sample
Ram B. Bhagat

Technical Report No. TR 88-015

December 1988

Supported by:
Naval Sea Systems Command

L. R. Hettche, Director
Applied Research Laboratory

Approved for public release; distribution unlimited

UNCLASSIFIED
SECURITY CLASSIFICATION OF THIS PAGE

AD-A205 717

REPORT DOCUMENTATION PAGE

1a REPORT SECURITY CLASSIFICATION UNCLASSIFIED	1b. RESTRICTIVE MARKINGS
2a SECURITY CLASSIFICATION AUTHORITY	3 DISTRIBUTION / AVAILABILITY OF REPORT Approved for public release; distribution unlimited
2b DECLASSIFICATION / DOWNGRADING SCHEDULE	
4 PERFORMING ORGANIZATION REPORT NUMBER(S) TR 88-015	5. MONITORING ORGANIZATION REPORT NUMBER(S)
6a NAME OF PERFORMING ORGANIZATION Applied Research Laboratory 6b OFFICE SYMBOL (If applicable) ARL	7a. NAME OF MONITORING ORGANIZATION Naval Sea Systems Command
6c ADDRESS (City, State, and ZIP Code) P.O. Box 30 State College, PA 16804	7b. ADDRESS (City, State, and ZIP Code) Department of the Navy Washington, DC 20362
8a NAME OF FUNDING / SPONSORING ORGANIZATION Naval Sea Systems Command 8b OFFICE SYMBOL (If applicable) NAVSEA	9. PROCUREMENT INSTRUMENT IDENTIFICATION NUMBER N00024-85-C-6041
8c ADDRESS (City, State, and ZIP Code) Department of the Navy Washington, DC 20362	10. SOURCE OF FUNDING NUMBERS PROGRAM ELEMENT NO. / PROJECT NO / TASK NO. / WORK UNIT ACCESSION NO.

11. TITLE (Include Security Classification)
FABRICATION OF UNIDIRECTIONAL FIBER REINFORCED 6061 ALUMINUM ALLOY USING HIGH PRESSURE SQUEEZE CASTING

12 PERSONAL AUTHOR(S)
P.J. Sample and R.B. Bhagat

13a TYPE OF REPORT	13b TIME COVERED	14. DATE OF REPORT (Year, Month, Day)	15. PAGE COUNT
M.S. Thesis	FROM _____ TO _____	December 1988	117

16 SUPPLEMENTARY NOTATION

17 COSATI CODES			18 SUBJECT TERMS (Continue on reverse if necessary and identify by block number)
FIELD	GROUP	SUB-GROUP	aluminum castings, aluminum alloys, squeeze casting, fiber-reinforced metal castings. (JES)

19 ABSTRACT (Continue on reverse if necessary and identify by block number)

Aluminum Alloy castings have been successfully reinforced with unidirectional graphite fibers. The reinforced castings were fabricated using an innovative technique known as high pressure squeeze casting. Previously, squeeze casting has been recognized as a superior metal forming method. The materials fabricated in this study demonstrate the ability of squeeze casting to achieve good fiber distribution and infiltration without the need for pretreatment of the fibers. There was very little observed chemical reaction between the graphite fibers and the aluminum in the ascast condition. The strength of the reinforced castings increased with increasing fiber volume fraction, although the strengths were generally less than those predicted by rule of mixtures. The tensile strengths ranged from 120 MPa for fiber volume fractions of 5 percent to 52 percent, respectively. A model was derived to explain the experimental

20 DISTRIBUTION / AVAILABILITY OF ABSTRACT ☒ UNCLASSIFIED/UNLIMITED ☐ SAME AS RPT. ☐ DTIC USERS	21. ABSTRACT SECURITY CLASSIFICATION UNCLASSIFIED
22a NAME OF RESPONSIBLE INDIVIDUAL	22b. TELEPHONE (Include Area Code) / 22c. OFFICE SYMBOL

DD FORM 1473, 84 MAR — 83 APR edition may be used until exhausted. All other editions are obsolete.

SECURITY CLASSIFICATION OF THIS PAGE
UNCLASSIFIED

data based mainly on the assumption that the interfacial bond between the fiber and the matrix was relatively weak compared to the strength of the fiber itself. Other properties of the castings were also examined including microhardness, stiffness and damping capability. In addition, a second model was developed using finite element methods to describe the transient thermal behavior of the molten aluminum during the squeeze casting process.

ABSTRACT

Aluminum Alloy castings have been successfully reinforced with unidirectional graphite fibers. The reinforced castings were fabricated using an innovative technique known as high pressure squeeze casting. Previously, squeeze casting has ben recognized as a superior metal forming method. The materials fabricated in this study demonstrate the ability of squeeze casting to achieve good fiber distribution and infiltration without the need for pre-treatment of the fibers. There was very little observed chemical reaction between the graphite fibers and the aluminum in the as-cast condition. The strength of the reinforced castings increased with increasing fiber volume fraction, althougn the strengths were generally less than those predicted by rule of mixtures. The tensile strengths ranged from 120 MPa to 310 MPa for fiber volume fractions of 5 percent to 52 percent, respectively. A model was derived to explain the experimental data based mainly on the assumption that the interfacial bond between the fiber and the matrix was relatively weak compared to the strength of the fiber itself. Other properties of the castings were also examined including microhardness, stiffness and damping capability. In addition a second model was developed using finite element methods to describe the transient thermal behavior of the molten aluminum during the squeeze casting process.

TABLE OF CONTENTS

LIST OF TABLES

LIST OF FIGURES

ACKNOWLEDGEMENTS

I would like to acknowledge the support and direction of my thesis advisor, Dr. Ram Bhagat, which has been instrumental in all the aspects of the preparation of this investigation. His hard work and perseverance are greatly appreciated. I would also like to acknowledge the invaluable assistance provided by Edward Smith, Lance Harbison, David Berkoff, Mark Rutherford, Jill Paulick and Jack Chisholm. The aforementioned all devoted a great deal of their valuable undergraduate time, for which I am very grateful. I wish them all the very best in their future endeavors. Further, I would like to acknowledge the assistance of Nagesh Sonti in the use the finite element program he developed. Finally, this work is dedicated to my parents, Marjorie and William. I thank them for their love and support.

Chapter 1

INTRODUCTION

1.1 High Pressure Squeeze Casting

Squeeze casting as a metal forming process was first developed over 40 years ago in the USSR [1]. Since that time it has attracted the interest of researchers in India [2,3], Japan [4-7], the United Kingdom [8-10] and the United States [11-14]. Squeeze cast metals offer much improved mechanical properties over conventional gravity cast metals and are comparable to those of forged wrought-alloys [14]. This is principally due to the improved micro-structural characteristics of squeeze cast metals and the absence of porosity and voids in the castings. The improved micro-structure is a direct result of the rapid solidification of the molten metals. Figure 1 shows the effect of pressure on the solidification of an Al-12Si alloy that was studied by Chatterjee and Das [8]. The rate of solidification of metals is significantly increased due to the effects of the pressure. First, the pressure acts to increase the effective rate of heat transfer by as much as an order of magnitude [11]. Next, the pressure forces the metal into almost perfect contact with the die wall which virtually eliminates contact resistance to heat transfer [8,15]. Finally, the pressure increases the characteristic melting temperature of materials that expand upon melting as predicted by the Clausius-Clapeyron equation [16].

Squeeze cast metals have been developed for use in a number of commercial applications including many in the automobile

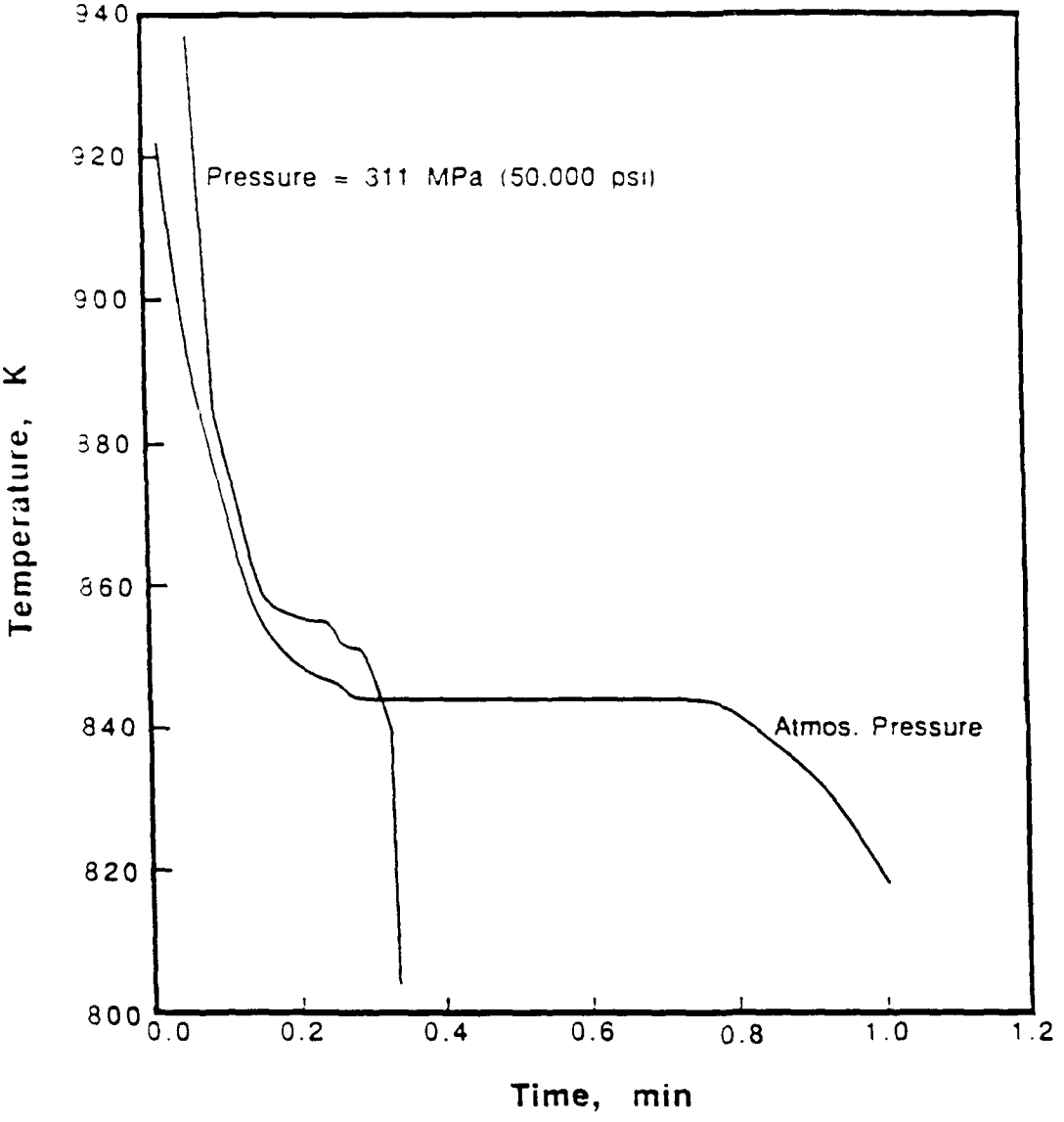

Figure 1. Solidification curves for Al-12Si alloy demonstrating the effect of pressure [8]

ndustry. There are a number of advantages to using squeeze casting over other metal forming techniques. Squeeze casting offers the ability to produce intricately shaped components and the strength and integrity of the castings rival those of forged materials. Figure 2 shows a comparison between two typical aluminum forging alloys that have been gravity cast, squeeze cast, squeeze cast and heat treated and forged and heat treated. In both cases, squeeze cast metals have significantly higher tensile strength than the respective gravity cast counterparts. Heat treating of the squeeze cast aluminum produces a material with tensile properties at least as great as the forged and heat treated aluminum. The squeeze cast Al-7Si alloy has a tensile strength 15% higher than the forged material in similar heat treatment conditions.

The strengthening of metals that have been squeeze cast has been shown to be a function of the casting pressures used [4,8]. The relationship between casting pressure and tensile strength can be seen in Figure 3 for three aluminum casting alloys. A normalized tensile strength is used in order to show the behavior of different alloys as a function of pressure. The normalized tensile strength is defined as the tensile strength at pressure P, S(P), divided by the tensile strength of that same alloy cast at atmospheric pressure, S_o. Casting pressures ranging from 100 to 150 MPa can be seen to produce significant increases in the tensile strength of the aluminum alloys. Still higher pressures result in higher strengths but the effect is less significant.

From the above one can see that squeeze casting is a very promising metal forming technique. Perhaps, however, the most

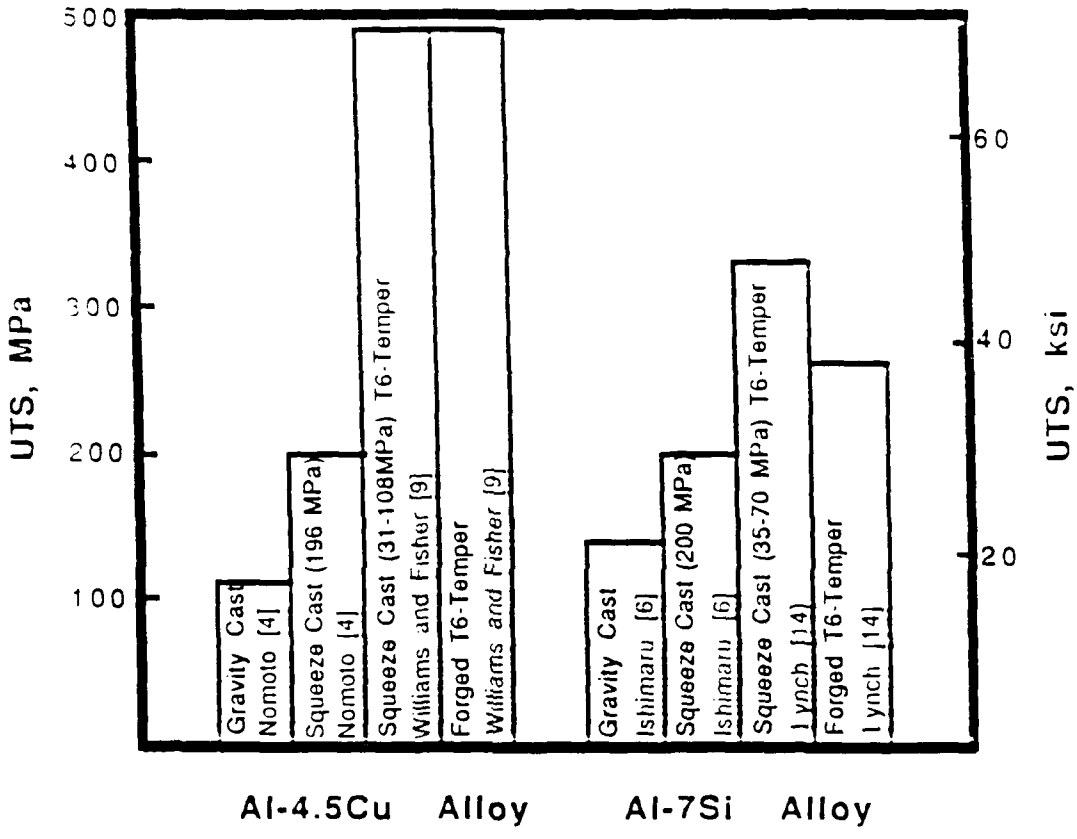

Figure 2. Comparison of tensile strength for two aluminum alloys formed by different processes

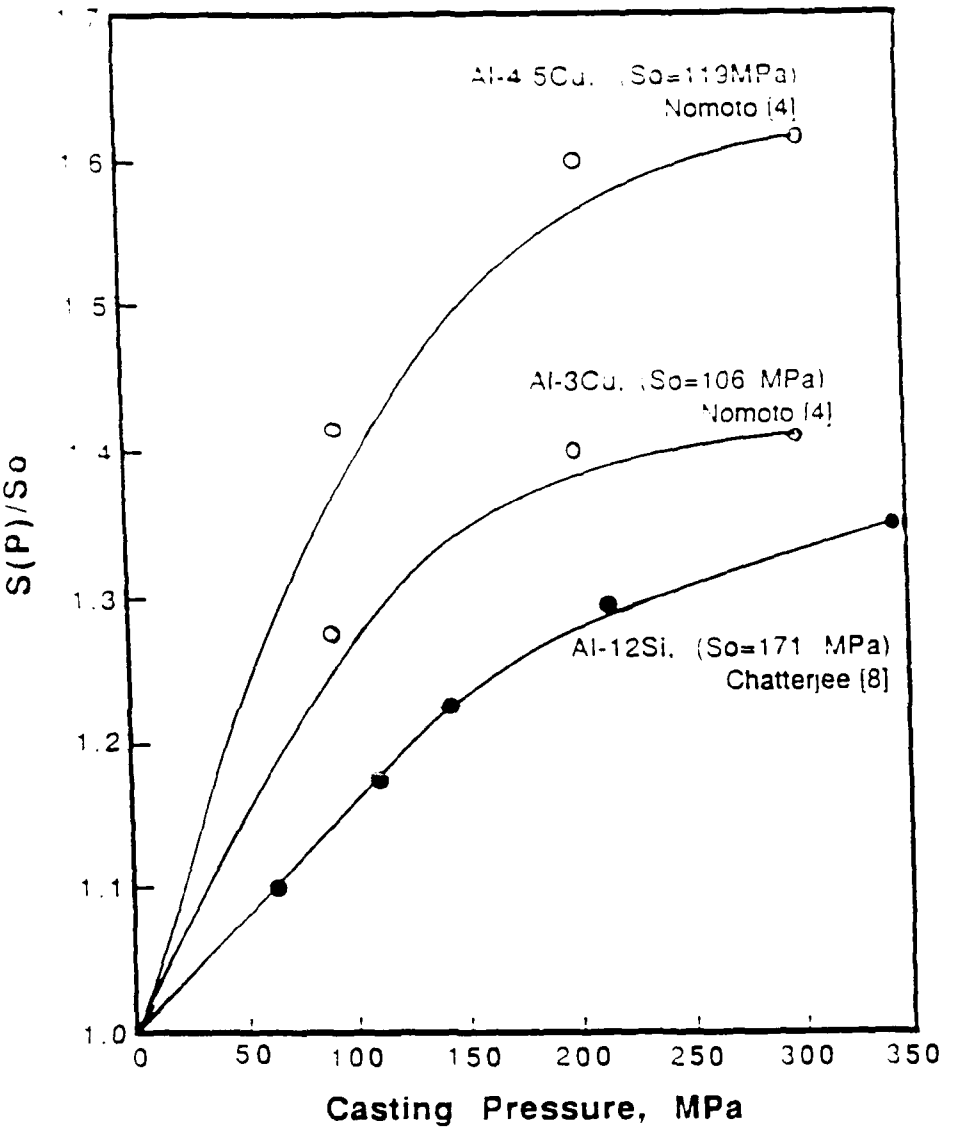

Figure 3. Effect of pressure on tensile strength of aluminum. Normalized tensile strength defined as the tensile strength of alloy cast at pressure, P, divided by strength of alloy cast at atmospheric pressure.

exciting prospects for high pressure casting lie in the fabrication of fiber reinforced metal components.

1.2 Fabrication of Fiber Reinforced Metals

Fiber reinforced metals offer a number of very attractive physical and mechanical properties. A partial list is given in Table 1.

The principal concern of these materials to date has been the relatively high cost of manufacturing. Some of the more common processing techniques are liquid metal infiltration and P/M hot pressing or diffusion bonding.

Liquid metal infiltration involves infiltrating the fiber reinforcement with molten metal. The metal is infiltrated into a fiber preform, often with the assistance of vacuum or low to moderate pressure. However, most liquid metals do not spontaneously wet the ceramic fibers used as reinforcement. For example, the Gr/Al system is a common composite system where liquid aluminum will not spontaneously wet the graphite fibers. Therefore the fibers require a coating or pre-treatment of some type in order to promote wetting. Typical coatings [17-19] include Ni, TiB, K_2TiF_6 and K_2ZrF_6. Sodium treatments have also been shown effective in promoting wetting of graphite fibers by molten aluminum [18]. The disadvantages of liquid metal infiltration lie in the limited ability to form complicated shapes and more importantly in the relatively long liquid metal to fiber contact times. These contact times more often can result in composites with less than optimal physical and mechanical properties through the degradation

Table 1. Some of the advantages of fiber reinforced metals

• Over Non-Reinforced Metals Higher specific strengths and stiffnesses Orthotropic properties allowing for the tailoring of composite to design specifications Improved damping (noise control)
• Over Fiber Reinforced Plastics Better high temperature properties Lower sensitivity to moisture Higher electrical and thermal conductivity
• Over Fiber Reinforced Ceramics Better fracture toughness -- more reliable

of the fibers by the molten metal and excess chemical reaction between the fibers and the matrix metal. This is particularly a problem with graphite fiber and aluminum matrix. The degradation of graphite fibers in aluminum was studied by Kohara and Muto [20]. Their study showed a decrease of 10 to 50% in the strength of graphite fibers (especially PAN fibers) that had been exposed to molten aluminum for times less than 5 minutes. The effect of chemical reaction on the strength of fiber reinforced metals can be seen in the Gr fiber reinforced aluminum studied by DeLamotte [17]. In this study, it was explained that the Ni coating that was used reacted with the Al to form a brittle inter-metallic compound at the fiber/matrix interface. It was further theorized that the brittle interface was unable to absorb the energy released by weak point failures in the fibers and redistribute the load among the remaining fiber segments resulting in premature failure of the reinforced aluminum.

Powder metallurgy hot pressing, on the other hand, is very costly and cumbersome for fabricating fiber reinforced metals. Fiber to matrix bonding is achieved by a sluggish solid state diffusion process at high temperatures for extended periods of time. These process conditions, namely, temperature, pressure and time allow densification of powder matrix and also can result in an excessive reaction between fiber and matrix. As described above, the excessive reaction is undesirable when fibers are used as reinforcement in metals. A trade-off between these two diametrically opposed requirements; the densification of the powder metal and the minimization of the fiber/matrix reaction, leads to

ess than expected values for the physical and mechanical properties of the materials. In addition, fibers exposed to the temperature, pressure and time of processing are invariably degraded. Hot pressing is also unsuitable for metals with continuous fiber reinforcement because of damage or breakage to the fibers. Hot pressing powders also results in poor distribution of the fibers throughout the metal. Therefore, hot pressing is often not commercially attractive.

Another fabrication technique to be discussed here is high pressure squeeze casting. In this case, squeeze casting as a metal forming technique mentioned at the beginning of this chapter can be modified to assist in the infiltration of fiber reinforcement. The advantages of squeeze casting can be directly related to its applicability to fabrication of fiber reinforced metals. The rapid rate of solidification results in minimal contact time between the fibers and the molten metal. This results in very little chemical reaction between the fibers and the matrix in the as-cast condition allowing for the tailoring of the interface during post casting processing. Also the pressure forces the metal to infiltrate the fibers, eliminating the need for pre-coating of the fibers [21,22]. Finally, with innovative preforming techniques squeeze casting offers the opportunity to fabricate planar random or unidirectional fiber reinforced near-net shape components at a reasonable expense. Recognizing the potential that high pressure squeeze casting possesses as a process for the fabrication of fiber reinforced metals and the limited amount of work available to date, there is a need for further investigation. This thesis will employ squeeze

casting process for the fabrication of fiber reinforced metals. The objectives and scope of this investigation follow.

1.3 Objectives and Scope of Investigation

The main objective of this investigation was to fabricate unidirectional fiber reinforced metals using high pressure squeeze casting.

The physical and mechanical properties including damping of the fabricated materials will also be studied along with a characterization of the fiber matrix interface. A model will also be developed for the transient thermal behavior of the process using finite element analysis.

The next chapter will describe the method developed to produce fiber reinforced metals using high pressure squeeze casting. Chapter 3 will outline the the finite element technique used to model the thermal behavior of the process. The testing procedures used for the fabricated materials will be discussed in Chapter 4 followed by the results and discussion in Chapter 5. Following Chapter 5 will be the conclusions from this study and recommendations for future research.

Chapter 2

FABRICATION PROCEDURES

In this chapter, a description of the process developed for the casting of fiber reinforced metals will be provided. The equipment and materials will be discussed first followed by the casting procedures.

2.1 Equipment and Materials

The following two sections will describe the equipment, the matrix and fiber materials and the unidirectional fiber preforming technique used to cast the reinforced metals.

2.1.1 Equipment

The equipment used for the casting of reinforced metals included a furnace for melting the metal, a metallic die and a hydraulic press, along with some minor accessories.

The furnace used to melt the metal had a maximum temperature of 1870 K (2900° F) and had no provision for atmospheric control. Temperature inside the furnace was regulated by an automatic on/off controller which maintained a user determined set-point.

The principal die used in this investigation was a 70 mm (2.7 inch) internal diameter circular die. A schematic drawing of this die is given as Figure 4. The die was made from 1040 steel. The die wall was case hardened to a maximum value of 56 on the Rockwell-C

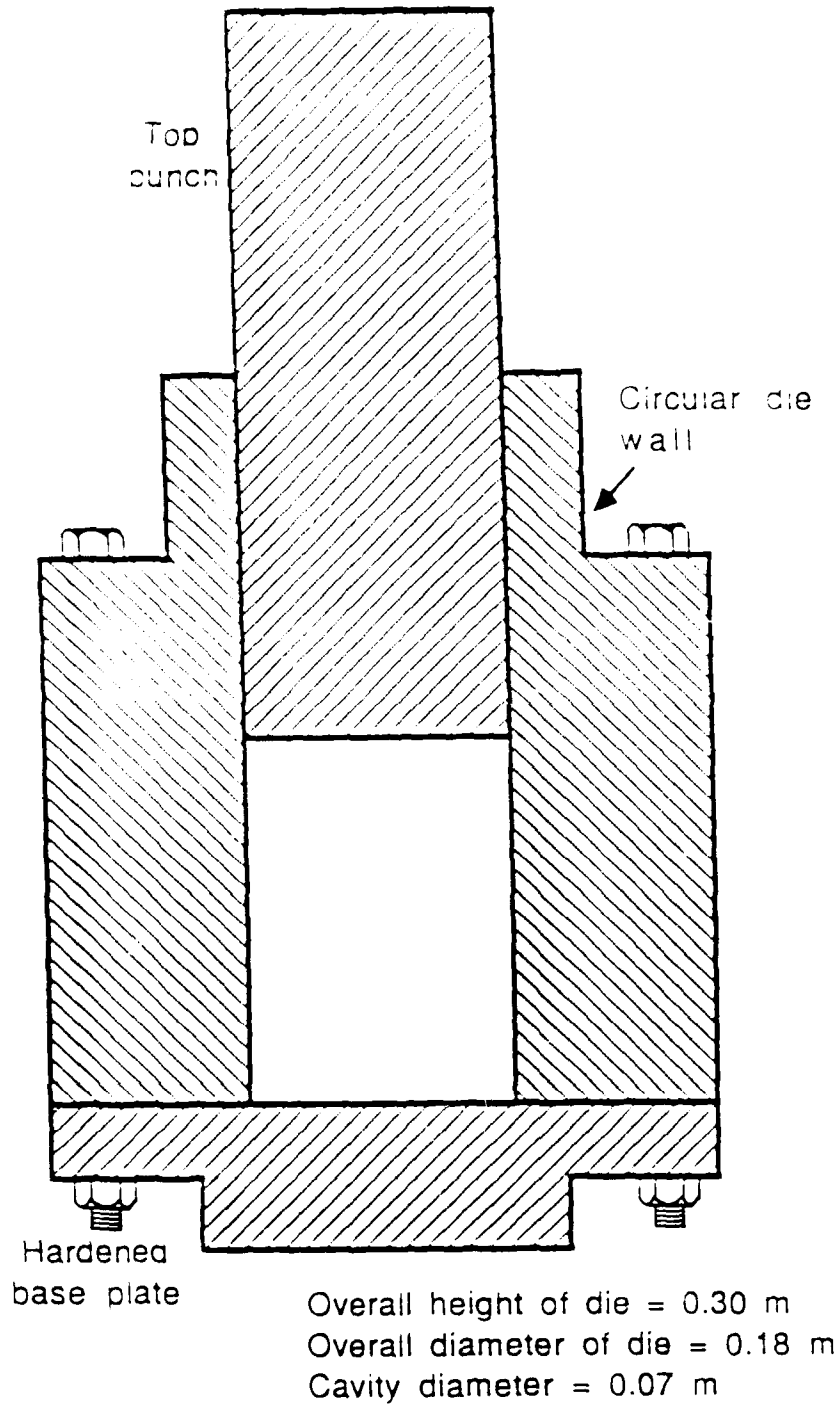

Figure 4. Primary die used for casting 70 mm fiber reinforced metal disks

scale to a depth of approximately 2.5 mm (0.1 inch). The base plate was also heat treated to the same specifications from the top surface of the plate. Likewise, the punch was also case hardened. The clearance between the punch and the die walls was small (0.025 mm--0.001 inch) so that when the pressure was applied, the molten metal was confined but the gases produced by the vaporization of the organic binders on the fibers were allowed to escape. The top surface of the base plate was ground smooth so that there would be a minimal amount of gap between base plate and the die wall. The die wall was secured to the base plate by high strength steel bolts.

A second die was used for casting of larger specimens. The internal diameter of this second die was 114 mm (4.5 inch). The materials and case hardening specifications for the second die were the same as those for the 6.9 cm (2.7 inch) die. A drawing of the 114 mm (4.5 inch) die is shown in Figure 5.

The pressure was applied through a 1779 kN (200 ton) hydraulic press. The load applied by the press was controlled by an adjustable pressure release valve. The load on the punch was calibrated as a function of the hydraulic pressure on the cylinder head. The calibration curve is given as Figure 6. Once the curve was established, the load on the punch could be found directly from the indicated hydraulic pressure.

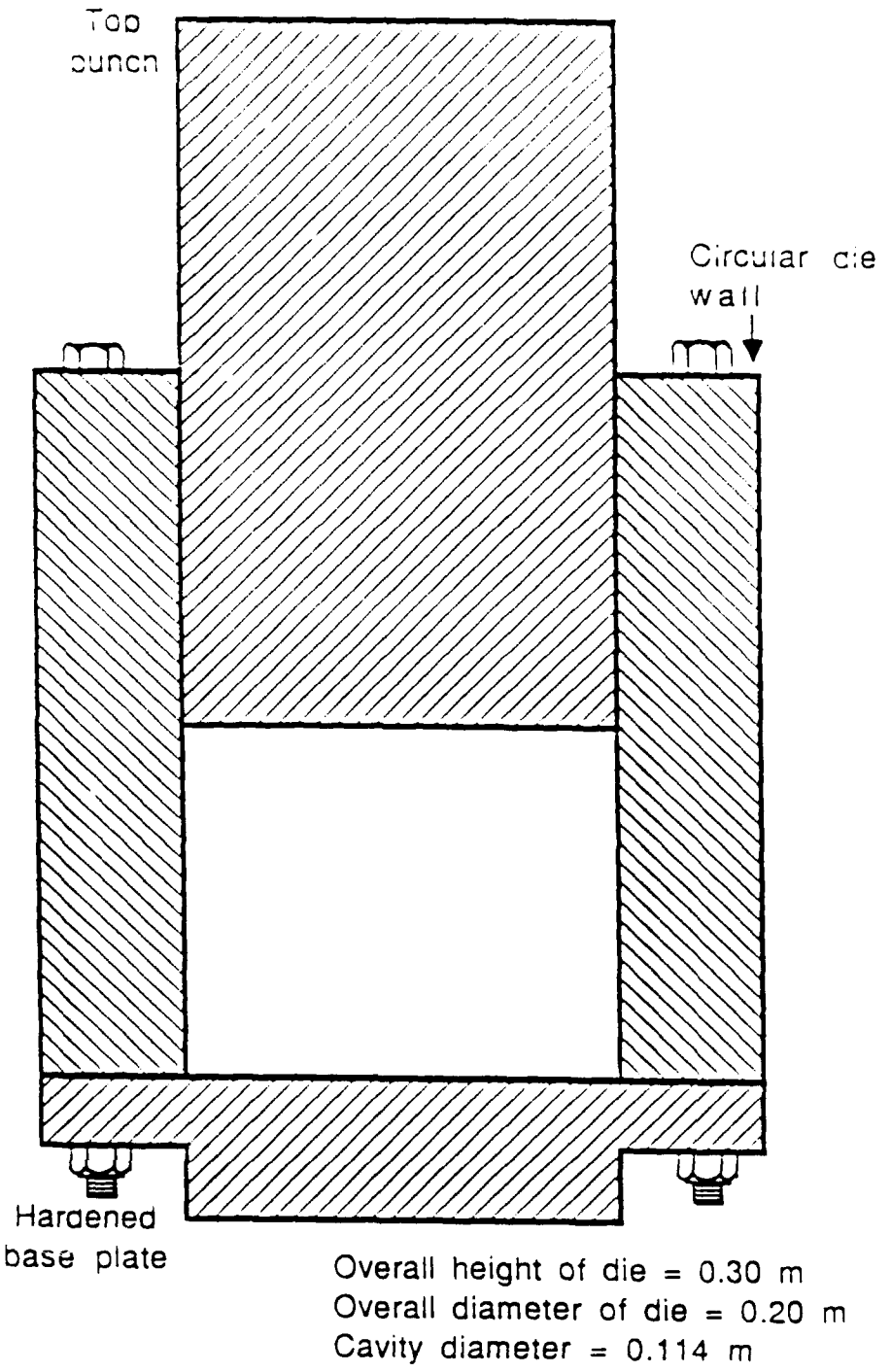

Figure 5. Die used for casting 114 mm diameter fiber reinforced metal disks

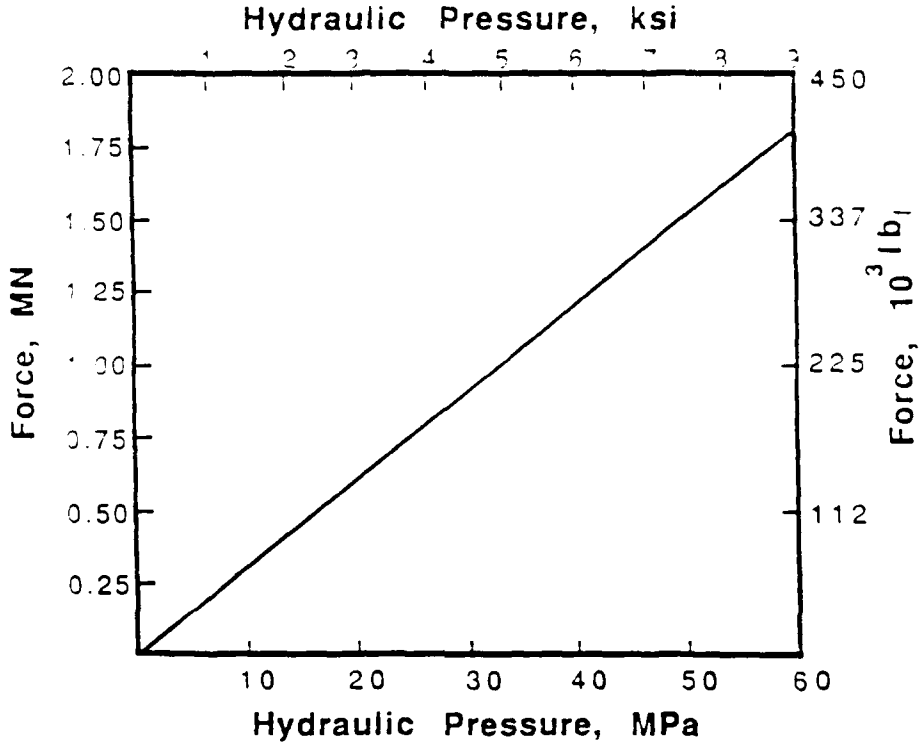

Figure 6. Calibration curve relating hydraulic pressure on the cylinder head to the applied load on the die punch

2.1.2 Materials

The matrix material used in this investigation was 6061 aluminum. The composition of this alloy and its physical and mechanical properties can be found elsewhere [23].

Graphite fibers were used to reinforce the aluminum matrix. Three forms of carbon/graphite fibers were used: graphite fiber tows containing approximately 2000 filaments each, sheets of Ni-coated carbon fibers laid out in a planar random orientation and held together by an organic binder and sheets of uncoated carbon fibers also in a planar random orientation.

The tow fibers were pitch based Thornel P-55. The physical and mechanical properties for the graphite tow fibers and the planar random carbon fibers are given in Table 2.

In addition to the graphite fibers used in the principal investigation, SiC (Nicalon) fibers were used to reinforce 6061 aluminum. These unidirectional fiber reinforced castings were fabricated using the same procedures described in this chapter for the Gr/Al castings.

2.1.3 Unidirectional Fiber Preform

This section will describe the unidirectional fiber preform used to fabricate the unidirectional fiber reinforced aluminum castings. The main objective of the preforming process was to prepare a preform with the majority of the fibers laid out in a parallel direction. When attempts were made to infiltrate preforms made from only the tow fibers, the directionality of the fibers was not maintained and there was poor infiltration by the liquid metal.

Table 2. Physical and mechanical properties of graphite/carbon fiber used to reinforce the aluminum castings

Physical or Mechanical Property	P-55 Tow Graphite Fiber	Random Sheet Carbon Fiber
Tensile Strength, MPa (ksi)	2100 (310)	3100 (450)
Young's Modulus, GPa (Msi)	379 (55)	235 (34)
Specific Gravity	1.8	1.8
Net Weight	0.0004[a]	0.00003[b] 0.00001[c]

a. in g/mm
b. in g/mm^2 for bare carbon fibers
c. in g/mm^2 for Ni-coated carbon fibers

Therefore a preforming technique combining the tow fibers, the thin Ni-coated fibers and the thicker uncoated fibers was developed.

The fiber preform consisted of multiple layers of tow fibers sandwiched between sheets of the Ni-coated fibers. The thicker uncoated carbon fiber sheets were used at the outer surfaces of the preform. The purpose of these sheets being to facilitate the liquid metal in infiltrating the extreme layers of the preform. The number of layers in the preform was a function of the target fiber volume fraction. A graph of this relation is given in Figure 7. For example, a fiber preform consisting of a top and bottom half having 10 layers each, where a layer is distinguished by a row of parallel tow fibers, or a total of 20 layers will yield a casting with an overall fiber volume fraction equal to approximately 0.22. Note: If the preform contains 0 layers, the fiber volume fraction is not 0 due to the presence of the randomly oriented thick fiber sheets.

A typical fiber preform is illustrated in Figure 8. The ratio of the mass of fibers oriented in the direction of the applied load as a function of the target fiber volume fraction is given in Figure 9. Three-eighths of the fibers in the random sheets were assumed to be oriented parallel to the tow fibers. The 3/8 coefficient was from an empirical equation developed to predict the elastic modulus of randomly oriented fiber reinforced materials from the longitudinal and transverse moduli [24]. The curve in Figure 9 approaches an asymptote at around 94% of parallel fibers as the effects of the thick planar random fiber sheets at the top and bottom of the overall preform become negligible. As an estimate for overall fiber volume

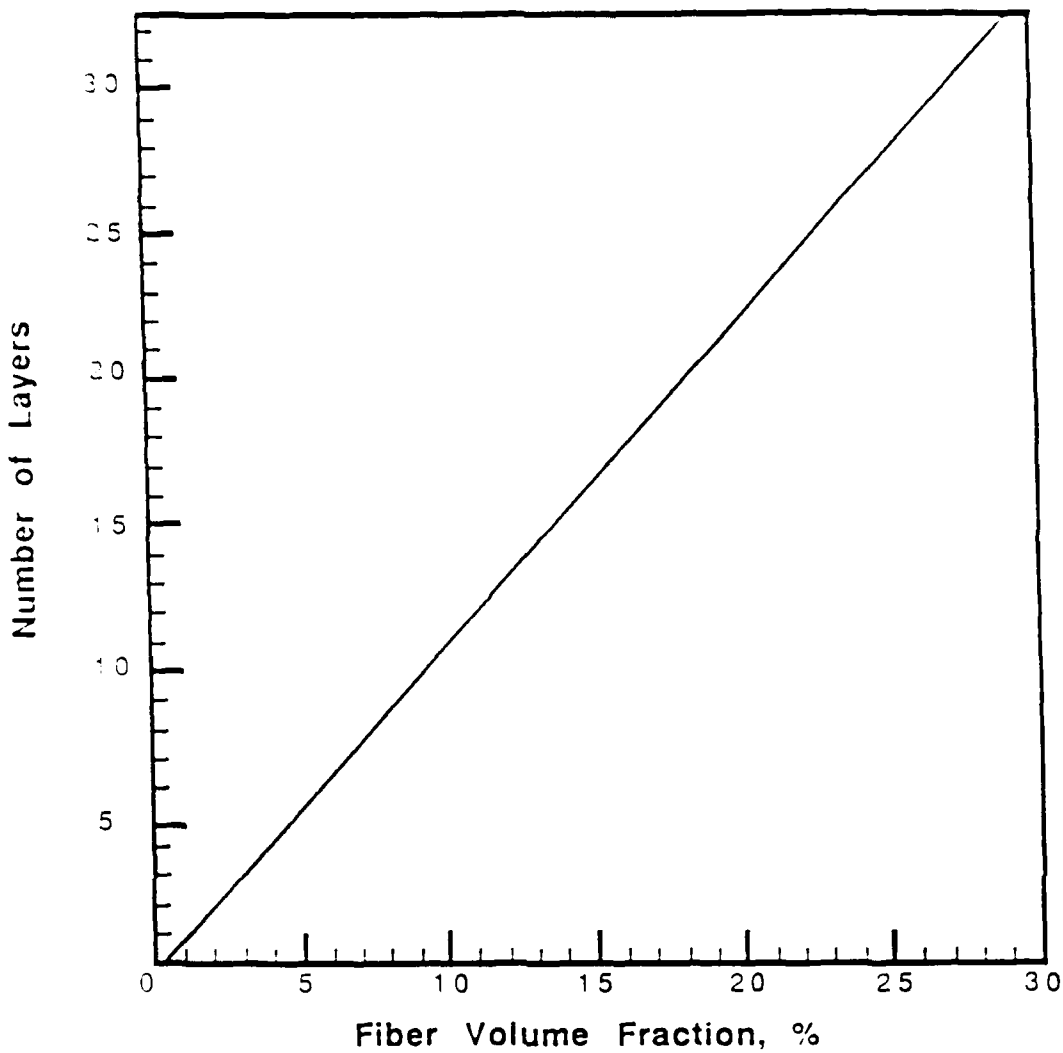

Figure 7. Layers in preform as a function of fiber volume fraction for a casting 70 mm in diameter and 3.2 mm thick. Fiber volume fraction is this figure is the overall fiber volume fraction which includes all the fibers, regardless of orientation. The number of layers is defined as the total number of stacked rows of parallel tow fibers.

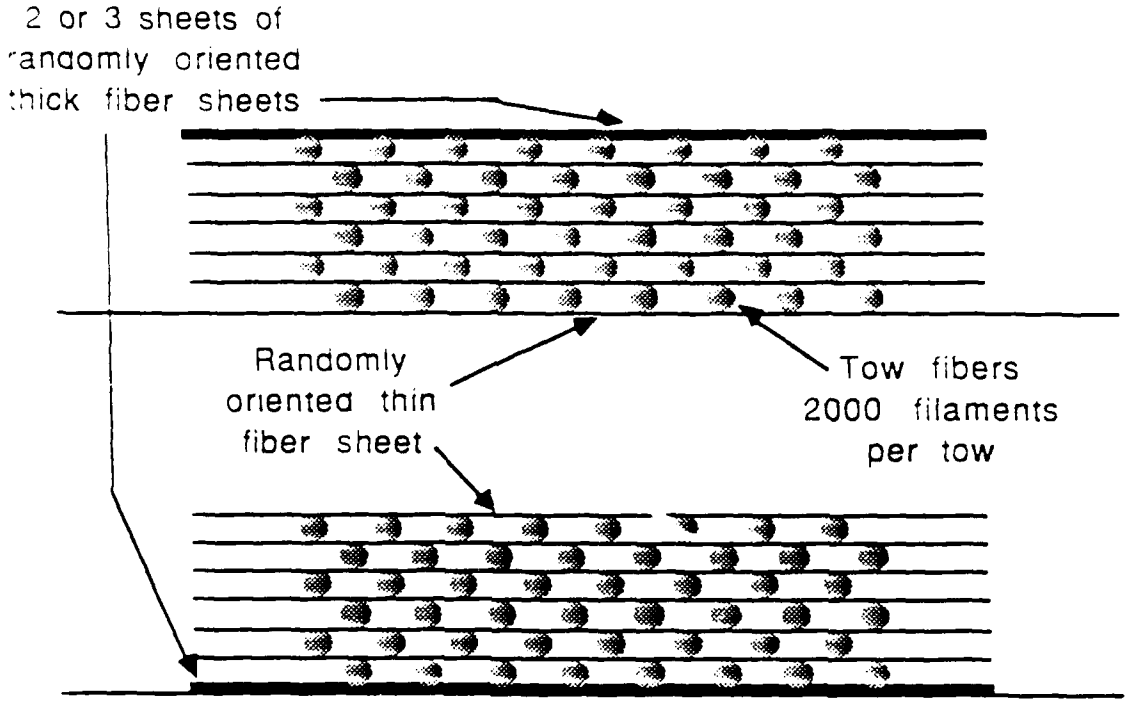

Figure 8. Schematic drawing of unidirectional fiber preform

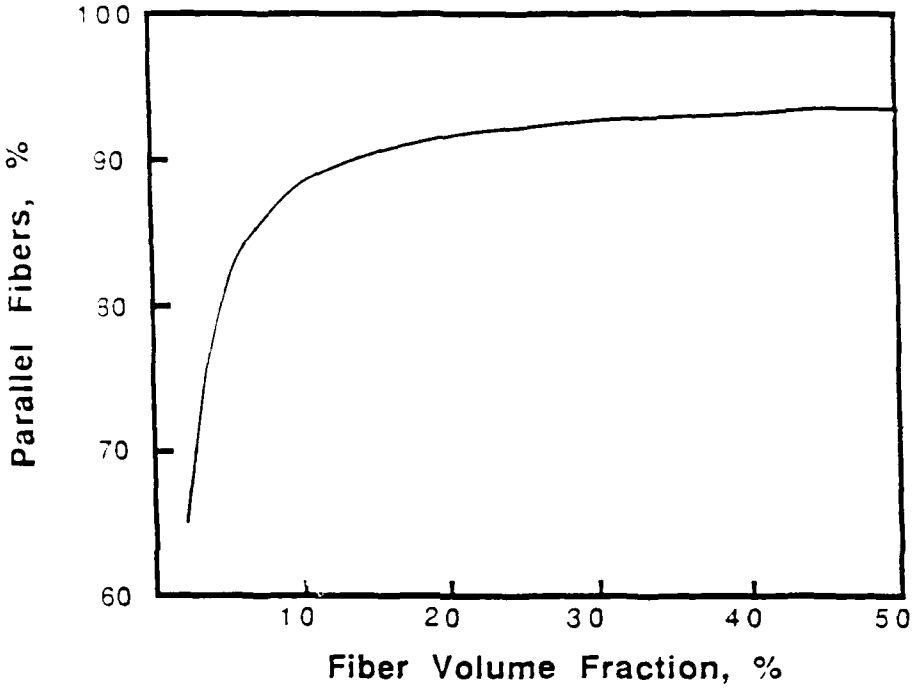

Figure 9. Percentage of fibers oriented parallel to one another as a function of the overall fiber volume fraction. The fiber fraction is the volume fraction of all the fibers regardless of orientation.

fractions above 0.15, the percentage of fibers oriented parallel to one another is assumed to be 90%.

2.2 Fabrication Procedures

The following paragraphs will describe the procedures used to fabricate carbon/graphite fiber reinforced aluminum using high pressure squeeze casting. Although the main objective of this work was to fabricate unidirectional reinforced castings, fabrication of planar random fiber reinforced castings was also performed in order to gain familiarity with the process and to provide data for comparison.

Whether planar random or unidirectional fibers were used, it was necessary prior to casting that the amount of metal and fibers be estimated for target fiber volume fraction. This calculation was based on the target fiber volume fraction and the size of the casting. For planar random fibers and for a selected target fiber volume fraction, the mass of fibers (M_f), in grams, required was calculated by

$$M_f = \pi r^2 t \rho_f v_f \qquad (1)$$

Where: v_f = target fiber volume fraction

ρ_f = density of fibers, g/mm^3

r = radius of circular die, mm

t = thickness of casting to be fabricated, mm

The mass of metal (M_m), in grams, was calculated directly using equation 2.

$$M_m = \pi r^2 t \rho_m (1-V_f) \quad (2)$$

Where: ρ_m = density of metal, g/mm^3

The target fiber volume fraction for unidirectional reinforced castings was used to determine the number of layers in the unidirectional preform that was required. To obtain a desired volume fraction of fibers oriented parallel to one another, that fiber volume fraction was divided by the appropriate ratio obtained from Figure 9. This adjusted fiber volume fraction then represented the overall fiber volume fraction which included both the tow fibers and the planar random fibers. Once the overall fiber volume fraction was determined the number of layers required in each of the two fiber preform was obtained from Figure 7.

The squeeze casting process consisted of three stages: the basic fiber and matrix material preparations, the pre-casting preparations of the die and the casting.

The basic fiber and matrix preparations consisted mainly of determining the proper amounts of each required and melting the metal. Also required was that the planar random fiber sheets be cut to the appropriate sizes and/or that the unidirectional fiber preforms be made.

Prior to casting, the die was cleaned and assembled. A carefully machined graphite disk was placed into the die at the

bottom of the cavity in order to form a liquid metal tight seal at the bottom of the die. One-half the total amount of fibers were also placed into the die prior to casting.

Casting of the metal consisted of pouring the molten aluminum which had been heated to a temperature of approximately 1200 K (1700 °F) into the prepared die and then adding the remaining fibers followed by a second graphite disk and the die punch. The actual temperature used was somewhat lower for the planar random reinforced castings and somewhat higher for the unidirectional reinforced castings. This was a result of the higher packing density of the tow fibers thus making them more difficult to infiltrate. The optimum temperature used was the lowest possible while still achieving complete infiltration in order to minimize the solidification time for the metal.

Once all the materials and the punch were in the die, the pressure was applied. The typical casting pressure used was 350 MPa (50 ksi). Although successful infiltration was achieved at lower pressures, the high pressure was chosen, again due to the desire to minimize the metal solidification time. A cross-section view of the die cavity just prior to the application of the pressure is given in Figure 10.

2.3 Heat Treatment of Castings

As the composites fabricated with the above procedures were optimized so as to have as little interfacial reaction as possible, it was expected that their strengths would not be as high as they might be with a relatively strong interfacial bond. Some

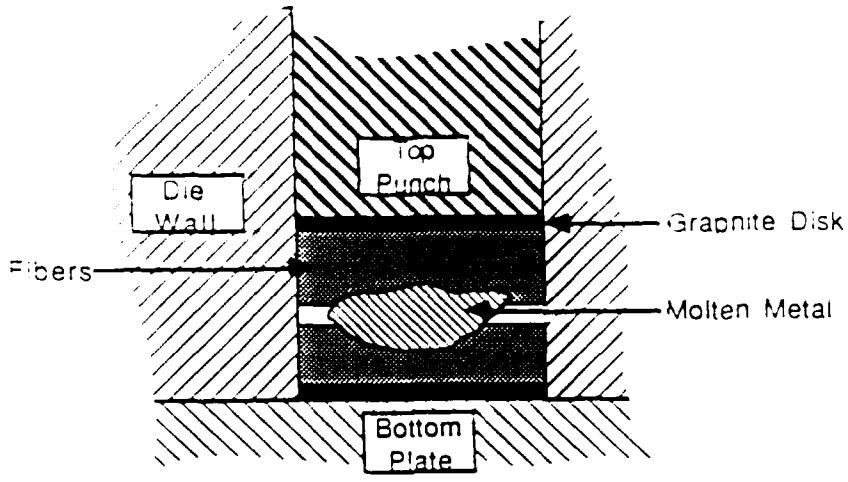

Figure 10. Cross-section view of die cavity just prior to application of pressure

chemical reaction between the fibers and the matrix can improve the strength of the fiber/matrix bond, thus improving the ability of the matrix to transfer the load to the reinforcing fibers.

From preliminary experiments, where the Gr/Al castings were simply heated to 825 K (1025 °F) for times ranging from 3 hr. to 240 hr. (high temperature heat treatment), it was found that it was necessary to heat the aluminum into the liquid region (very high temperature heat treatment) in order to effect a reaction between the carbon and the aluminum. This was accomplished by heating an as-cast composite specimen in a rectangular die that was heated to several degrees above an experimentally determine solidus temperature for the 6061 aluminum used in this study. The setup used in the present investigation is shown in Figure 11. After a predetermined period of time (several seconds to a few minutes), high pressure was applied to the die in order to increase the solidification temperature of the aluminum alloy, as described by the Clausius-Clapeyron equation; this solidified the aluminum alloy and essentially stopped further reaction. The die was then allowed to cool in air and the pressure was released when the temperature fell below the solidus temperature.

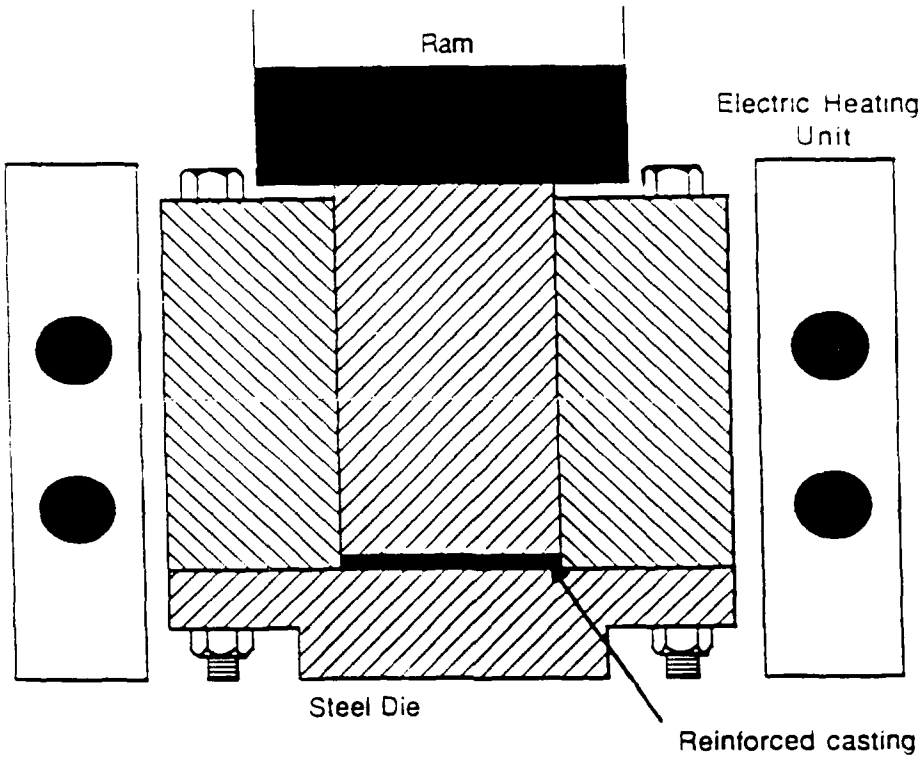

Cavity Dimensions - 5.7 cm x 3.5 cm

Die Outside Diameter - 15.2 cm

Figure 11. Heat treatment set-up for Gr/Al casting to effect controlled reaction between the fibers and the matrix

Chapter 3

Transient Thermal Analysis of Squeeze Casting Process

3.1 Introduction to Thermal Analysis

In the squeeze casting process described in the previous chapter, the application of high pressure has two effects on the casting process. First, it facilitates the infiltration of the molten metal around the fibers. Second, it dramatically reduces the solidification time of the liquid aluminum, thus reducing the amount of reaction between the fiber and the aluminum matrix. Pressure reduces the solidification time by reducing the contact resistance at the die wall and by effectively increasing the solidification temperature of the molten matrix metal.

The modelling of solidification of metals and alloys is complex because several parameters including temperature dependent thermal properties, convection and radiation heat losses, phase change and the apparent increase in thermal conductivity due to the convection of the molten metal need to be considered. Closed form solution for solidification processing is practically impossible. However, these problems can be handled rather simply with the use of numerical methods such as finite element method (FEM) [25].

A recently developed finite element based computer program, THERM [26], was modified to carry out thermal analysis of the squeeze casting process, the code required some modifications. In the squeeze casting process there is some degree of heat loss from all sides of the die. Fortunately, since the die cavity was round, it

could be modelled using axisymmetric elements which allowed the two-dimensional THERM program to model the three-dimensional problem.

There are three main objectives of the analysis contained in this chapter: a. To modify the FEM program THERM in order to give it axisymmetric element capability. b. To solve some test problems from the literature in order to demonstrate the accuracy of the solution results obtained using THERM. c. To perform a computational analysis of the solidification of aluminum during the squeeze casting process for fabricating reinforced castings.

3.2 THERM

THERM is a finite element code originally designed to study one- and two-dimensional transient heat transfer. Present element capability of THERM includes quadrilateral elements with 4 to 8 nodes. There are also provisions for temperature dependent thermal properties, convection and radiation heat losses, phase change and the apparent increase of thermal conductivity due to convection of the molten metal.

THERM uses a variational formulation derived from the governing partial differential equation,

$$\frac{\partial}{\partial x}\left(k_x \frac{\partial T}{\partial x}\right) + \frac{\partial}{\partial y}\left(k_y \frac{\partial T}{\partial y}\right) = \rho C \frac{\partial T}{\partial t} \qquad (3)$$

Where : x, y = coordinate axes

k_x, k_y = thermal conductivities in the x and y

directions, respectively

T = temperature

ρ = density of the metal

C = specific heat capacity of the metal

t = time

The boundary and initial conditions are that there is no internal heat generation per unit volume. By the incorporation of additional terms convection and radiation heat losses are also allowed.

The derivation of the final equation requires an explanation of variational calculus which is too involved for this study and may be found elsewhere [26], therefore the result is simply presented as Equation 4.

$$\int \delta(\underline{T}'^{T})\ {}^{t+\Delta t}\underline{k}\ {}^{t+\Delta t}\underline{T}'\ dV) = \int \delta T^{S}\ {}^{t+\Delta t}q^{S}\ dS) - \int \delta T\ {}^{t+\Delta t}(\rho C)\ {}^{t+\Delta t}\left(\frac{\partial T}{\partial t'}\right) dV - \int \delta T^{S}\ {}^{t+\Delta t}h_{c}\ {}^{t+\Delta t}(T^{S}-T_{a})\ dS - \int \delta T^{S}\ {}^{t+\Delta t}h_{r}\ {}^{t+\Delta t}(T^{S}-T_{a})\ dS \qquad (4)$$

Where: $$\underline{T}'^{T} = \left\{ \frac{\partial T}{\partial x}\ \frac{\partial T}{\partial y} \right\}$$

$$\underline{k} = \begin{Bmatrix} k_{x} & 0 \\ 0 & k_{y} \end{Bmatrix}$$

On the right-hand side of Equation 4, the first term represents the surface heat input. The second term deals with the volumetric heat capacity and the third and fourth terms represent the convection and radiation heat losses, respectively.

The numerical solution to Equation 4 is obtained, using Euler's backward implicit time integration [25]. Equation 4 is nonlinear as a result of the temperature dependent thermal properties. The non-linearities are handled by first linearizing the thermal properties and then applying a modified Newton-Raphson iterative solution method [25].

Input of the thermal properties, initial conditions and the calculation parameters are accomplished by reading the values into the main program from a separate formatted input file. The format required for this input file follows.

3.3 Input File Format

The format of the input file used to input the material thermal properties, initial conditions and the calculation parameters is provided in this section in tabular form. A description of each entry for every column is given on a line by line basis. Related groups of lines are given in each of Tables 3 through 8.

Table 3. General information to define system and to provide guidelines for calculations used in THERM

Line 1		
Column	**Variable**	**Entry**
1-10	NELEM	Number of elements
11-20	NNODE	Number of node
21-30	NTIMES	Total number of time steps
31-40	NITERS	Maximum number of iterations per time step
41-50	NG	Number of Gauss points to be used in calculations
51-60	NMATL	Total number of materials
61-70	NLUMP	Lumped parameter matrix (0 = consistent, 1 = lumped)
71-80	NCHECK	Trial run to check mesh generation 1-mesh and material property check only 0-run entire program

Table 3. Continued

Line 2		
Column	**Variable**	**Entry**
1-10	THICK	Thickness of elements (0.0 for axisymmetric elements)
11-20	DELT1	Primary time step value
21-30	DELT2	Secondary time step value
31-40	TMELT	Melting temperature of molten material
41-50	TAMB	Ambient temperature
51-60	TINIT	Initial temperature
61-70	CONVCR	Convergence criteria for iterations
71-80	NPRINT	Print after how many time steps?

Table 4. Line defining welding parameters. Line is needed even if welding application is not required.

Line 1		
Column	**Variable**	**Entry**
1-10	XARC	Initial 'x' position of welding arc
11-20	XEND	Final 'x' position of welding arc
21-30	ZARC	Initial 'z' position of welding arc
		Set equal to 1.0 for no weld
31-40	ZEND	Final 'z' position of welding arc
41-50	POWER	Power input of welding arc
51-60	SPEED	Speed arc moves in the 'x' direction
61-70	RO	Initial radius of weld pool
		Set equal to 1.0 for no weld
71-80	EFF	Efficiency of weld input

Table 5. Material property information. This group of lines is repeated for each material.

Line 1		
Column	**Variable**	**Entry**
1-10	TS	Solidus temperature
11-20	TL	Liquidus temperature
21-30	HLAT	Latent heat
31-40	EMISS	Emissivity
41-50	CMULTP	Enhancement factor for convection of molten material
51-60	N(k)	Number of temperatures for which thermal conductivity values are to be given
61-70	N(C)	Number of temperatures for which heat capacity values are to be given
71-80	N(H)	Number of temperatures for which enthalpy values are to be given

Table 5. Continued

N(K) Lines		
Column	**Variable**	**Entry**
1-10	T(K)	Temperature at which k is to be given
11-30	K	Thermal conductivity, k, at T(K)
N(C) Lines		
1-10	T(C)	Temperature at which C is to be given
11-30	C	Heat capacity, C, at T(C)
N(H) Lines		
1-10	T(H)	Temperature at which H is to be given
11-30	H	Enthalpy, H, at T(H)

Table 6. Coefficient for convective heat transfer

Line 1		
Column	**Variable**	**Entry**
6-15	HC	Coefficient for convective heat transfer

Table 7. Element data

NELEM Lines		
Column	**Variable**	**Entry**
1-5	N	Element number
6-10	NDIFF	Difference in element numbers, used to generate element data
11-15	NE(N)	Defines boundary for convective heat transfer (See Figure 3.1)
16-20	MATL(N)	Material number?
21-25	NN(N)	Number of nodes used to define element (4-8)
26-30	NP(1)	Node point 1
31-35	NP(2)	Node point 2
36-40	NP(3)	Node point 3
41-45	NP(4)	Node point 4
46-50	NP(5)	Node point 5
51-55	NP(6)	Node point 6
56-60	NP(7)	Node Point 7
61-65	NP(8)	Node point 8

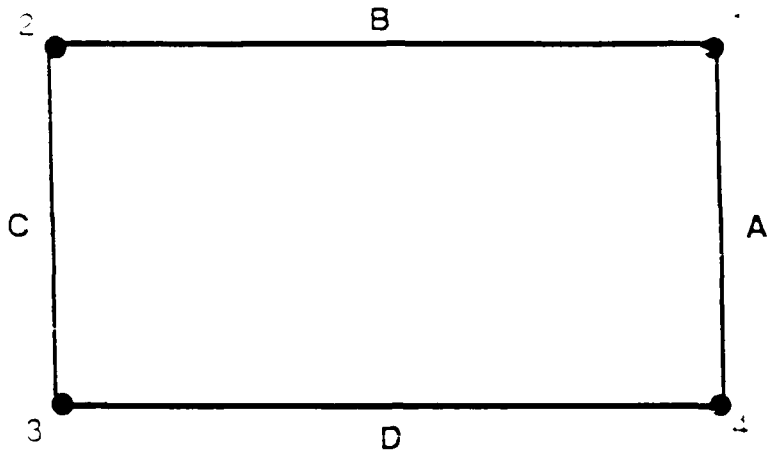

Input Value for NE Heat Transfer Face	
1	A
2	B
3	C
4	D
5	A and B
6	B and C
7	C and D
8	A and D

Figure 12. Convective heat loss boundary conditions

Table 8. Nodal data

NNODE Lines		
Column	**Variable**	**Entry**
1-5	N	Node number
5-10	NDIFF	Difference in node numbers, used to generate node coordinates
11-20	X(N)	'x' coordinate of node N
21-30	Y(N)	'y' coordinate of node N

3.4 Axisymmetric Analysis

The ability to model the round die cavity used for squeeze casting of fiber reinforced metals in the present investigation with axisymmetric elements allows for the prediction of the transient heat transfer behavior in the three-dimensional cavity using the two-dimensional program THERM. The axisymmetric elements, shown in Figure 13, are ring shaped elements with quadrilateral cross-sections. When using axisymmetric elements, the finite element mesh is specified for one-half of the specimen cross-section and these elements are essentially rotated 360 degrees to represent the entire specimen being modelled. Essentially the modification consisted of changing the thickness for each element from a constant number to a variable determined by the distance of that element from the center of the specimen being modeled. This puts the requirement on the input that 'x' must always be equal to 0.0 at the center of the specimen.

Test problems using the modified version of THERM are contained in the next section followed by a model to describe the squeeze casting process.

3.5 Test Problems

In this section, two test problems with established solutions will be set-up. The modified version of THERM will be used to solve these problems with the results presented in Chapter 5. The computed solutions will be compared to solutions from published literature.

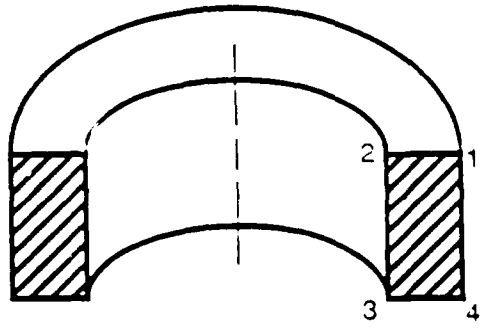

Figure 13. Typical axisymmetric element used in experimental model. Numbers represent each of four nodes at the corners of the quadrilateral cross-section.

3.5.1 One-Dimensional Heat Transfer Example

A 1.52 m x 0.30 m x 0.30 m cavity contains a material with properties specified in Table 9. The cavity is insulated on all sides except for one of the shorter sides. The rate of solidification of this material can be predicted using THERM. The finite element mesh used is shown in Figure 14. The exact solution for this problem was obtained from a study by Hsiao [27].

3.5.2 Two-Dimensional Heat Transfer Example

A 3.05 m square by 0.30 m deep cavity contains a metal having the properties specified in Table 10. There is convective heat loss from all sides of the cavity. Due to symmetry, one quarter of the cavity was modelled as shown in Figure 15. The position of the solid/liquid interface was predicted THERM. The literature solution of this problem also was obtained from the study by Hsiao [27].

3.6 Modelling Squeeze Casting Process

In the high pressure squeeze casting process for fabricating fiber reinforced metal casting, molten metal is poured into a metallic die containing one-half the total fiber reinforcement to be used. Immediately after pouring, the remaining fibers are placed into the die on top of the molten metal. The punch is then placed in the die and high pressure is applied until the metal has completely solidified.

This process is divided into three consecutive steps. Each of these steps is modelled independently with the final thermal conditions of the previous step being used as the initial conditions

Table 9. Material properties and initial conditions for one-dimensional test problem

Material Properties		
Solidus Temperature	T_S	532.6 K [499.5 °F]
Liquidus Temperature	T_L	533.4 K [500.5 °F]
Melting Temperature	T_m	533 K [500 °F]
Latent Heat of Fusion	H_L	3730 KJ/m³ [100 Btu/Ft³]

Thermal Conductivity, KJ/m(s)(K) [Btu/(Ft)(s)(°F)]	**Temperature,** K [°F]
6.2 [1.0]	assumed constant

Heat Capacity, KJ/m³ [Btu/Ft³]	**Temperature,** K [°F]
37.3 [1.0]	assumed constant

Enthalpy, KJ/m³ [Btu/Ft³]	**Temperature,** K [°F]
0.0 [0.0]	311 [100]
14,900 [399.5]	532.6 [499.5]
18,600 [499.5]	533.4 [500.5]
23,000 [619.0]	600.0 [620.0]

Initial Conditions		
Initial Temperature	T_i	600 K [620 °F]
Ambient Temperature	T_a	311 K [100 °F]
Coefficient for Convective Heat Transfer	h_c	12,900 KJ/m²(s)(K) [630 Btu/Ft²(s)(°F)]

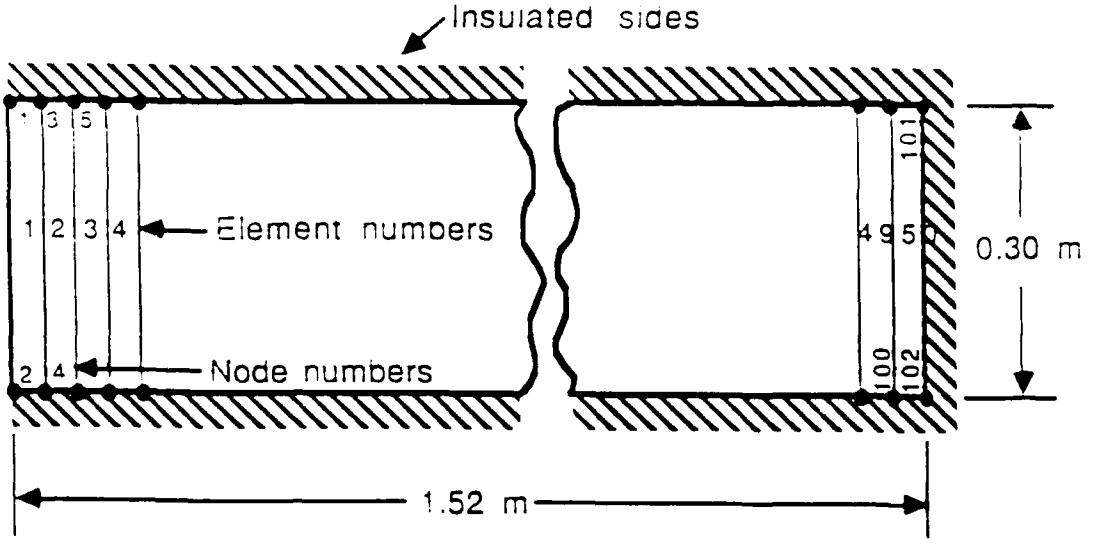

Figure 14. Finite element mesh used to model one-dimensional test problem. Heat loss is by convection from left side of cavity as drawn.

Table 10. Material properties and initial conditions for two-dimensional test problem

Material Properties		
Solidus Temperature	T_S	699 K [799 °F]
Liquidus Temperature	T_L	700 K [700 °F]
Melting Temperature	T_m	700 K [801 °F]
Latent Heat of Fusion	H_L	3730 KJ/m^3 [100 Btu/Ft^3]

Thermal Conductivity, KJ/m(s)(K) [Btu/(Ft)(s)(°F)]	**Temperature,** K [°F]
6.2 [1.0]	699 [766]
5.6 [0.90]	700 [801]

Heat Capacity, KJ/m^3 [Btu/Ft^3]	**Temperature,** K [°F]
37.3 [1.0]	assumed constant

Enthalpy, KJ/m^3 [Btu/Ft^3]	**Temperature,** K [°F]
0.0 [0.0]	311 [100]
26,000 [699]	699 [799]
39,000 [1049]	700 [801]
46,500 [1248]	1000 [811]

Initial Conditions		
Initial Temperature	T_i	811 K [1000 °F]
Ambient Temperature	T_a	311 K [100 °F]
Coefficient for Convective Heat Transfer	h_c	41 KJ/m^2(s)(K) [2.0 Btu/Ft^2(s)(°F)]

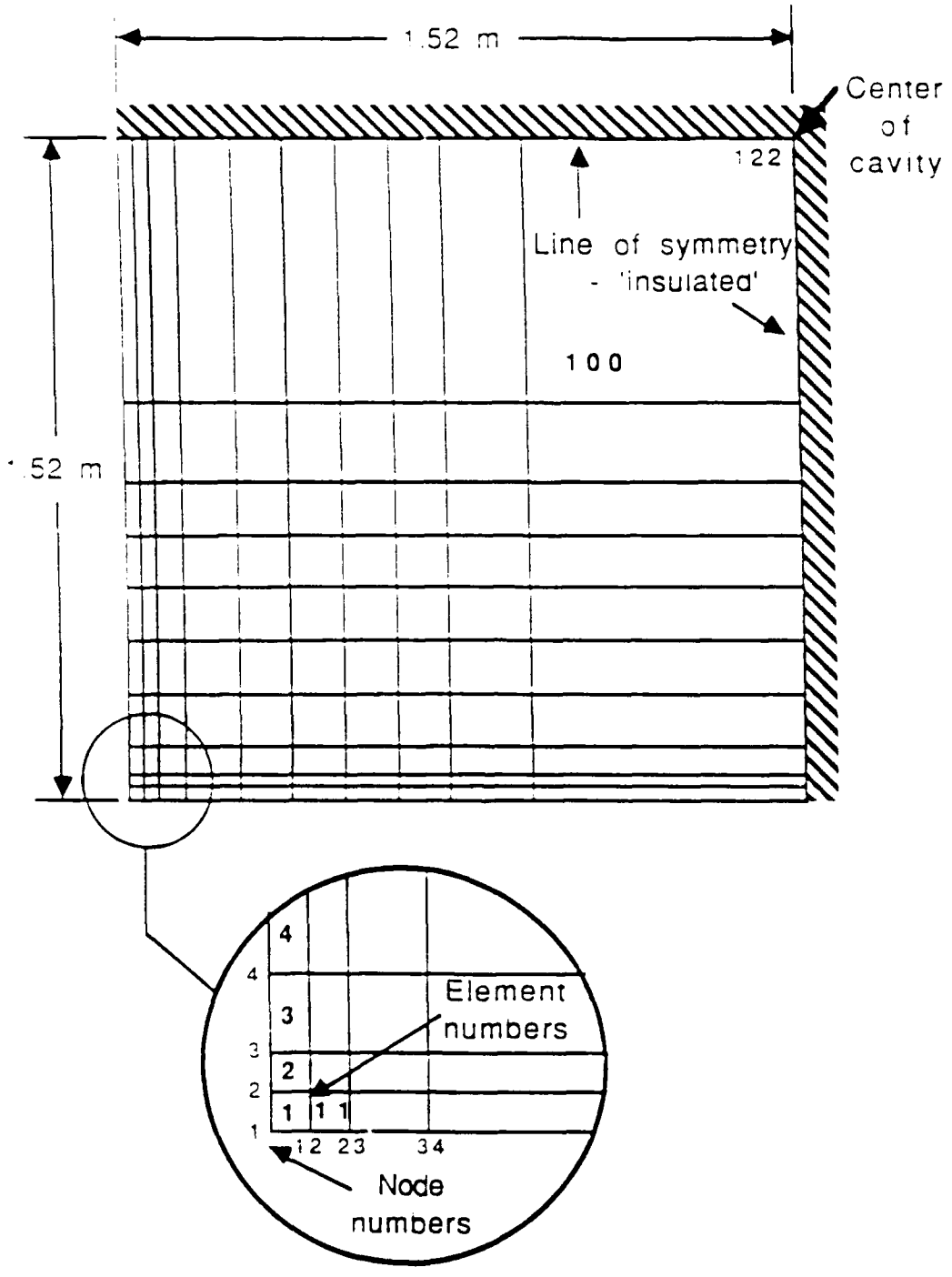

Figure 15. Finite element mesh used to model two-dimensional test problem. Heat loss is by convection from left-hand and near sides of cavity as shown.

for the next. The first step is defined as when the metal and all the fibers are placed in the die but the punch still has not been. The section modelled includes from the center of the molten metal to the top of the fibers as shown in Figure 16. Since no pressure has been applied yet, there is still a considerable amount of air surrounding the fibers and this is modelled as alternating layers of air and graphite with the air layers representing the greatest volume. In this step it is assumed that no infiltration has yet occurred. The input conditions for this step are contained in Table 11. Included are the thermodynamic properties for the three materials; aluminum, graphite and air and the initial conditions.

The second step is defined as when the punch has been placed into the die causing the fibers to compress but still the high pressure has not been applied so there still is no infiltration. The input for this step is the same for the first except that the initial temperature becomes the average temperature of the molten metal after 1.5 seconds in step 1. The mesh used in this step is also similar to that in the first with less volume of air. The actual mesh used is shown in Figure 17. This step is run for the equivalent of another 2 seconds of process time, and the average temperature of the molten metal is then used in the final step.

In the final step the high pressure has been applied and the the cavity no longer contains any air and the material is modelled as a combination of graphite and aluminum. The mesh used to model the final step is shown in Figure 18. The thermodynamic values for this material were calculated from equations available from the literature [24] and are given in Table 12. In order to simulate the

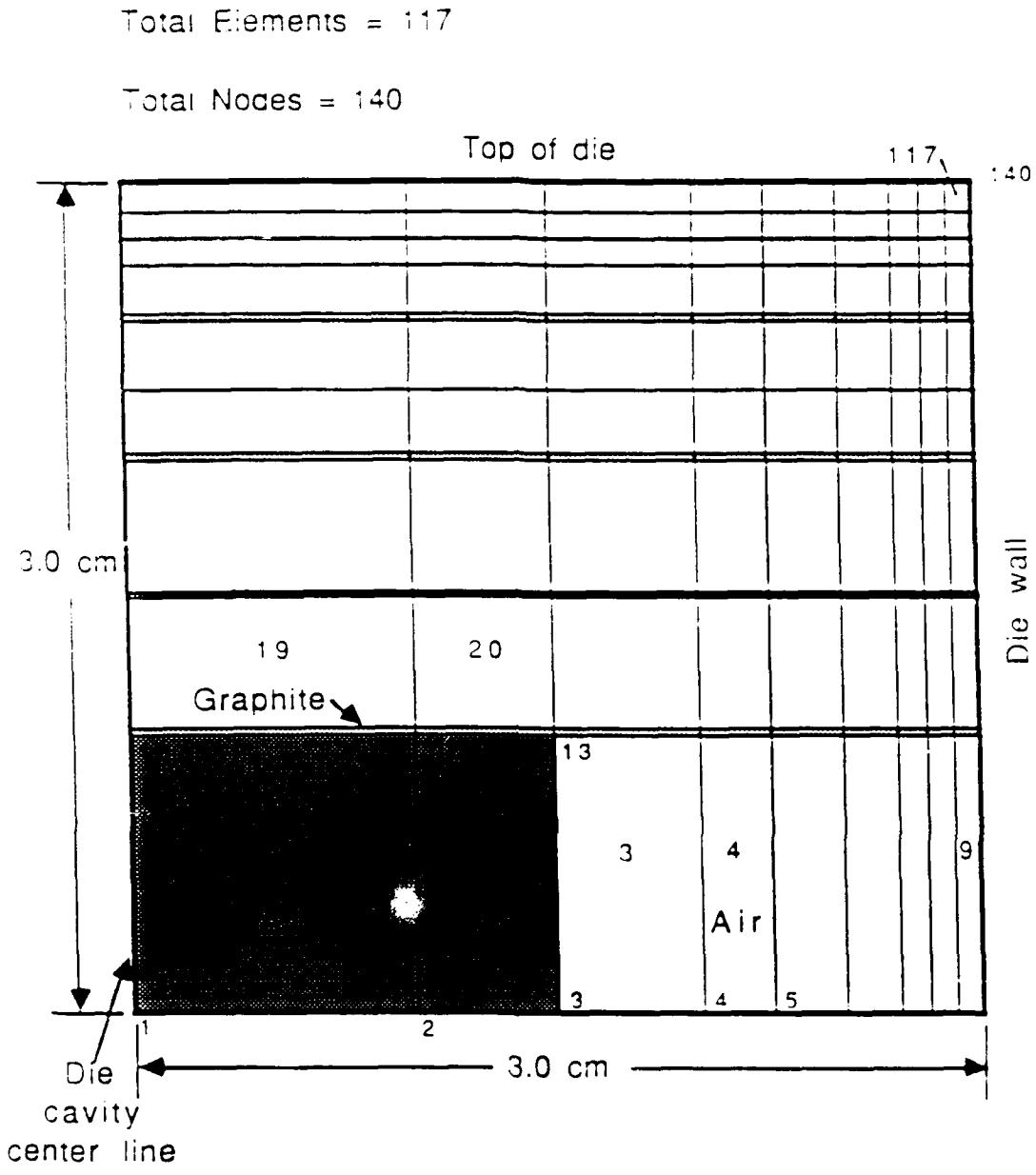

Figure 16. Finite element mesh used to model first step in experimental model. Fiber volume fraction equal to 30 percent. Heat loss is modelled as convective from top and right hand sides as drawn. Elements are quadrilateral axisymmetric.

Table 11. Thermodynamic properties of materials used in experimental model and initial conditions

Material Properties (Aluminum)	
Solidus Temperature T_S	855 K [1079 °F]
Liquidus Temperature T_L	925 K [1205 °F]
Melting Temperature T_m	925 K [1205 °F]
Latent Heat of Fusion H_L	1.1×10^6 KJ/m³K [16.4×10^3 Btu/Ft³°F]

Thermal Conductivity, KJ/m(s)(K) [Btu/(Ft)(s)(°F)]	Temperature, K [°F]
0.25 [0.040]	298 [77]
0.23 [0.036]	473 [329]
0.22 [0.035]	873 [1,112]
0.21 [0.034]	1,273 [1,832]
0.20 [0.032]	1,473 [2,192]

Heat Capacity, KJ/m³K [Btu/Ft³°F]	Temperature, K [°F]
2,400 [35.8]	293 [68]
2,800 [41.7]	673 [752]
2,900 [43.2]	1,073 [1,472]
2,900 [43.2]	1,473 [2,192]

Enthalpy, $\times 10^6$KJ/m³K [$\times 10^3$Btu/Ft³°F]	Temperature, K [°F]
0.0 [0.0]	293 [68]
1.1 [16.4]	673 [752]
3.3 [49.2]	1,073 [1,472]
4.5 [67.1]	1, 473 [2,192]

Material Properties (Graphite)	
Solidus Temperature T_S	> 2000 K
Liquidus Temperature T_L	> 2000 K
Melting Temperature T_m	> 2000 K
Latent Heat of Fusion H_L	0.45×10^6 KJ/m³K [6.7×10^3 Btu/Ft³°F]

Table 11. Continued

Thermal Conductivity, KJ/m(s)(K) [Btu/(Ft)(s)(°F)]	Temperature, K [°F]
0.050 [0.008]	293 [68]
0.100 [0.016]	773 [932]
0.092 [0.015]	973 [1,292]
0.050 [0.008]	1,473 [2,192]

Heat Capacity, KJ/m³K [Btu/Ft³°F]	Temperature, K [°F]
921 [13.7]	225 [-54.7]
2,500 [37.3]	500 [440]
3,100 [46.2]	1,000 [1,340]
3,600 [53.7]	1,500 [2,240]

Enthalpy, x10⁹KJ/m³K [x10³Btu/Ft³°F]	Temperature, K [°F]
0.0 [0.0]	293 [68]
0.45 [6.7]	473 [392]
2.14 [31.9]	973 [1,292]
4.31 [64.3]	1,473 [2,192]

Material Properties (Air)		
Solidus Temperature	T_S	5 K [-451 °F]
Liquidus Temperature	T_L	5 K [-451 °F]
Melting Temperature	T_m	5 K [-451 °F]
Latent Heat of Fusion	H_L	582 KJ/m³K [8.7 Btu/Ft³°F]

Thermal Conductivity, KJ/m(s)(K) [Btu/(Ft)(s)(°F)]	Temperature, K [°F]
2.6×10^{-5} [4.2×10^{-6}]	293 [68]
3.8×10^{-5} [6.1×10^{-6}]	498 [437]
5.9×10^{-5} [9.5×10^{-6}]	998 [1,337]
6.7×10^{-5} [11.0×10^{-6}]	1,198 [1,697]
7.5×10^{-5} [12.0×10^{-6}]	1,473 [2,192]

Heat Capacity, KJ/m³K [Btu/Ft³°F]	Temperature, K [°F]
1.2 [0.018]	assumed constant

Table 11. Continued

Enthalpy. KJ/m³K [Btu/Ft³°F]	**Temperature.** K [°F]
0.0 [0.0]	293 [68]
582 [8.7]	773 [932]
1,214 [18.1]	1,273 [1,832]
1457 [21.7]	1,473 [2,192]
Initial Conditions	
Initial Temperature T_i	1,473 K [2,192 °F]
Ambient Temperature T_a	293 K [68 °F]

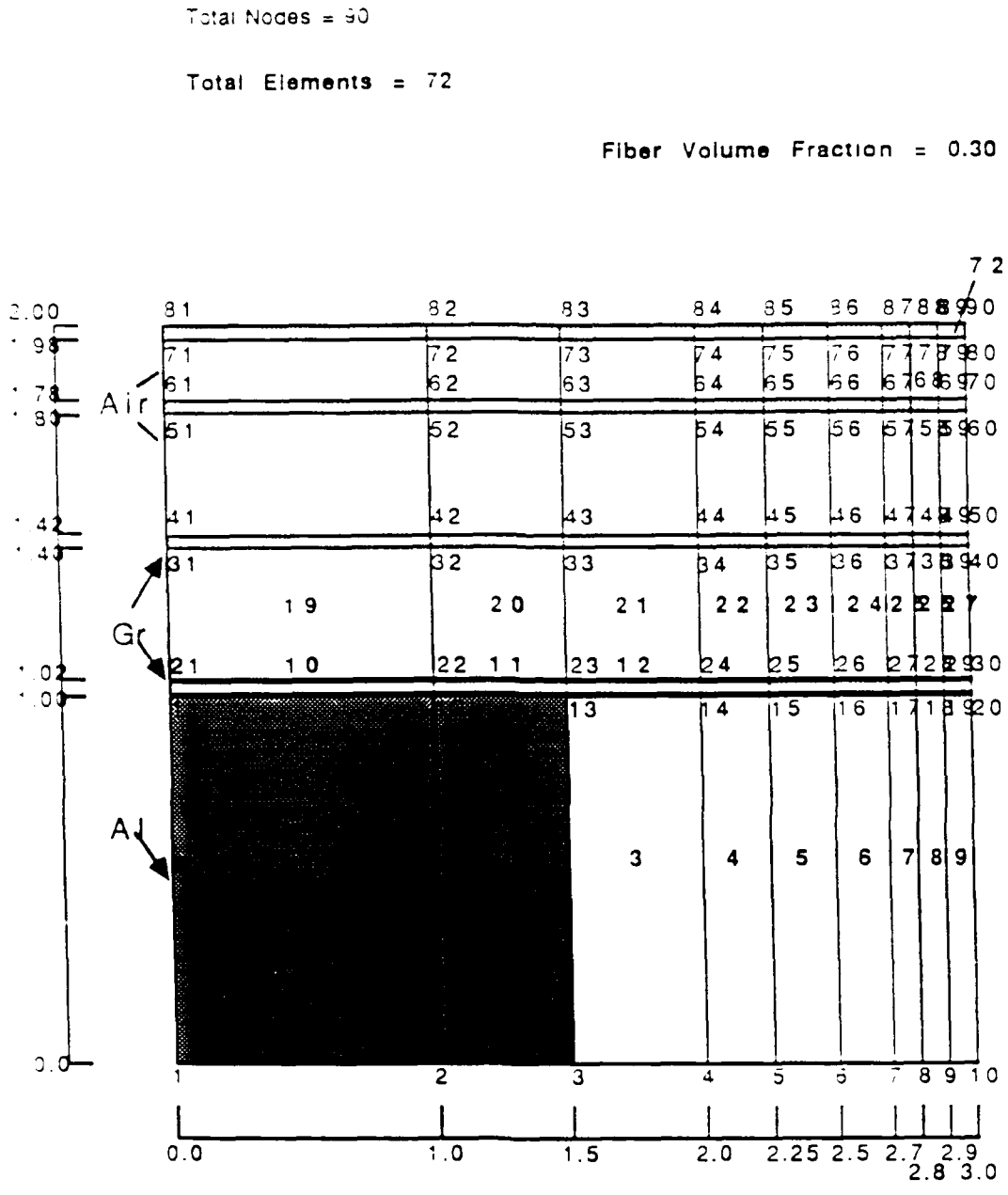

Figure 17. Finite element mesh used to model second step in experimental model. Heat loss is modelled as convective from top and sides of figure as drawn. Elements are quadrilateral axisymmetric.

effect of pressure on the heat transfer through the die wall , the reduction of contact resistance due to the pressure, the coefficient for convective heat transfer is increased a order of magnitude over the value used in steps 1 and 2. This is consistent with some experimental observations referenced [11] in Chapter 1 of this study which indicate an order of magnitude increase in the overall rate of heat transfer through a die wall when high pressure is applied rather than simple gravity casting.

The average temperature for the molten metal as a function of time in the three steps described above were then combined to give a representation of the transient thermal behavior of the process for fabricating fiber reinforced metal castings. This curve will be presented in Chapter 5 on results and discussion.

Although there are still factors in the solidification of molten metal castings with fiber reinforcement that are not addressed by this model, such as the effect of the fibers in providing nucleation sites, the model does cover the more significant areas and acts as a good starting point for further development.

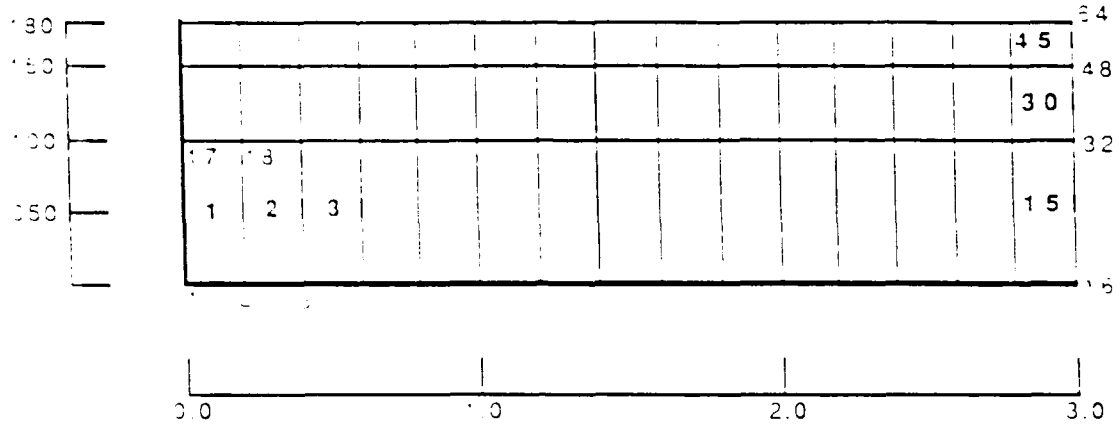

Figure 18. Finite element mesh used to model final step in experimental model. Heat loss is modelled as convective from the top and right hand side of the figure as drawn. Elements are quadrilateral axisymmetric.

Table 12. Theoretical thermodynamic properties for graphite fiber reinforced aluminum

Material Properties (Graphite/Aluminum)	
Solidus Temperature T_S	855 K [1079 °F]
Liquidus Temperature T_L	925 K [1205 °F]
Melting Temperature T_m	925 K [1205 °F]
Latent Heat of Fusion H_L	1.1x10^6 KJ/m^{3}K [16.4x10^3 Btu/Ft^3°F]

Thermal Conductivity, KJ/m/s/(K) [Btu/(Ft)/s/(°F)]	Temperature, K [°F]
0.19 [0.030]	298 [77]
0.18 [0.029]	873 [1,112]
0.16 [0.024]	1,473 [2,192]

Heat Capacity, KJ/m^{3}K [Btu/Ft^3°F]	Temperature, K [°F]
2,070 [30.8]	293 [68]
2,580 [38.5]	500 [440]
2960 [44.1]	1,000 [1,340]
3,110 [46.4]	1,500 [2,240]

Enthalpy, x10^{6}KJ/m^{3}K [x10^{3}Btu/Ft^3°F]	Temperature, K [°F]
0.0 [0.0]	293 [68]
1.11 [16.4]	673 [752]
2.95 [44.0]	1,073 [1,472]
[66.2]	1,473 [2,192]

Chapter 4

TESTING PROCEDURES

This chapter describes the procedures used to characterize the fabricated fiber reinforced castings.

The tests performed include tensile tests, micro-hardness tests and microscopic examinations. Also, measurements were carried out for evaluating the damping characteristics of the reinforced castings.

4.1 Procedures for Tensile Testing

Tensile tests were performed in order to characterize the tensile strength and stiffness of the fabricated reinforced castings. Tests were performed on an Instron machine. A controlled strain rate was maintained with a cross-head speed equal to 0.051 cm/min (0.020 in/min) for all tests. The load as a function of time for the test was recorded using a chart recorder. Self tightening wedge shaped grips were used to secure the specimens. These grips increased the gripping force as a function of the load on the specimens.

There were two similar types of test specimens used in the tensile tests. Both were a typical dog bone shape. The specimens used for the ultimate strength measurement had a narrower cross-section in order to promote a more uniform fracture in the gage length. The second type of dog bone shaped specimen had a

considerably wider cross-section in order to facilitate the mounting of a strain gage for determination of primary stiffness and fracture strains for the castings. The two types of tensile specimens are illustrated in Figure 19. The width of the gage length for the strength specimens and the stiffness specimens was approximately 0.64 cm (0.25 inch) and 1.27 cm (0.5 inch), respectively. Overall widths were approximately 1.27 cm (0.5 inch) and 1.90 cm (0.75 inch), respectively. The length of the specimens was the same of either type and was a function of the location from which the specimen was taken from the original casting. The variation can be seen in Figure 20. Gage lengths were consistently 2.54 cm (1.0 inch) for all specimens.

The specimens were cut using a high speed rotary tool with a 0.64 cm (0.25 inch) carbide tipped bit. This tool allowed cutting of the casting only in the direction parallel to the fiber reinforcement, thus minimizing any delamination of the casting prior to testing.

The ultimate fracture strength of the reinforced castings was measured by allowing the tensile test machine's cross-head to continuously pull the specimen at the specified speed. For stiffness measurement, the test specimens were loaded to a small fraction of their anticipated ultimate strength and a record was made of load versus the strain, indicated by the strain gage. Tests were performed one time only for each specimen. The fracture strain was measured by loading test specimens with strain gages all the way to fracture.

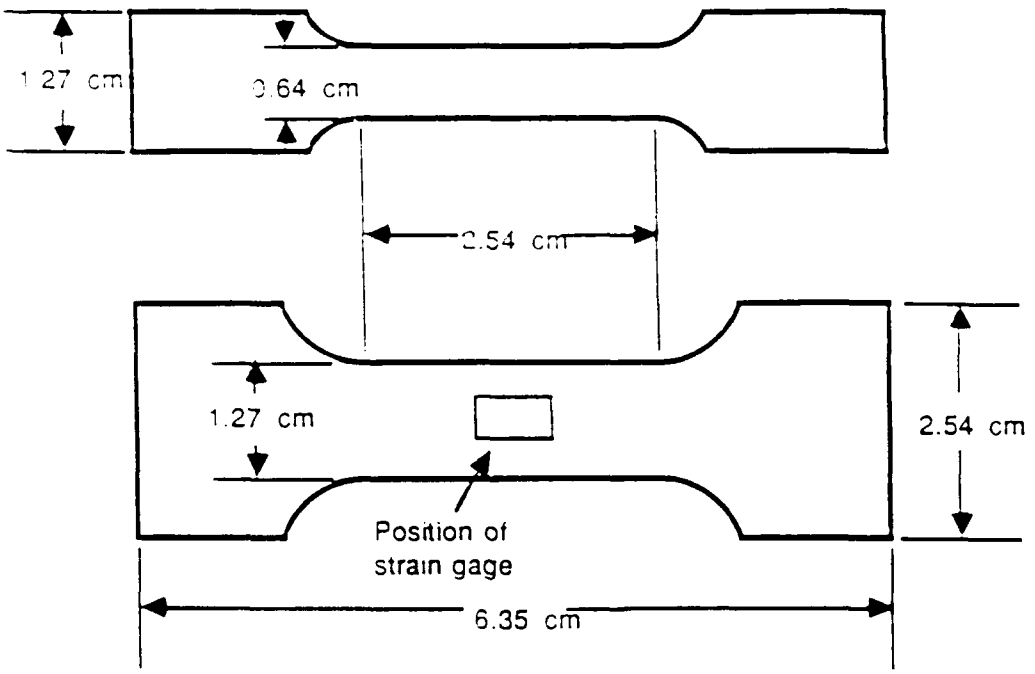

Figure 19. Two types of tensile test specimens used for the measurement of a.) tensile strength and b.) stiffness and fracture strain of fiber reinforced castings.

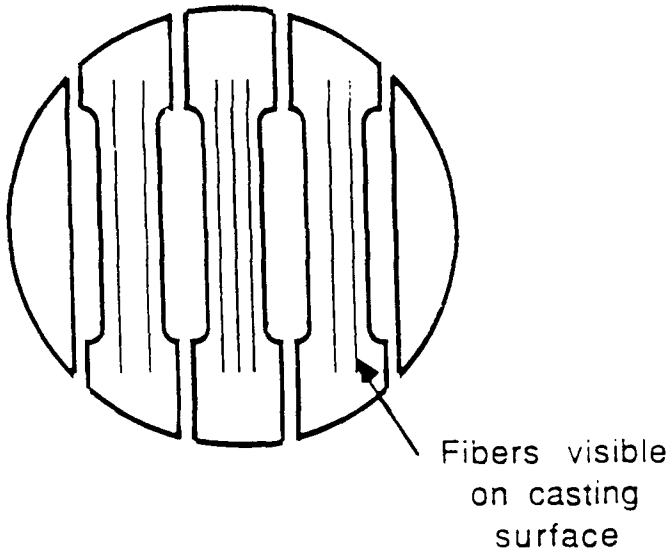

Figure 20. Schematic illustration of tensile specimens from unidirectional fiber reinforced casting showing relative location of specimens

4.2 Procedures for Determination of Microhardness

The microhardness of the squeeze cast 6061 Al matrix was determined using a Vicker's diamond indenter. The matrix was tested in four conditions: as-cast with no fiber reinforcement, fiber reinforced matrix that had been subjected to high temperature solid state heat treatment and fiber reinforced matrix that had been heat treated at a temperature above the experimentally determined solidus temperature.

The procedure for determining the Vicker's micro-hardness included measuring the diagonals of the diamond shaped indentation and using the average diagonal length and the applied load.

The micro-hardness is defined as:

$$\text{Vicker's hardness (HV)} = \frac{F}{A} \qquad (5)$$

Where F is the force applied to the indenter and A is the area of the indentation. An indentation is shown schematically in Figure 21. The shape is a regular pyramid with the the face angle assumed to be equal to the face angle of the indenter. The area of the indentation, A, is given by the following relationship:

$$A = \frac{2 \sin \frac{136°}{2}}{d^2} \qquad (6)$$

Where the face angle of the diamond is 136° and d is the average length of the diagonals. Substituting equation (6) into (5) yields

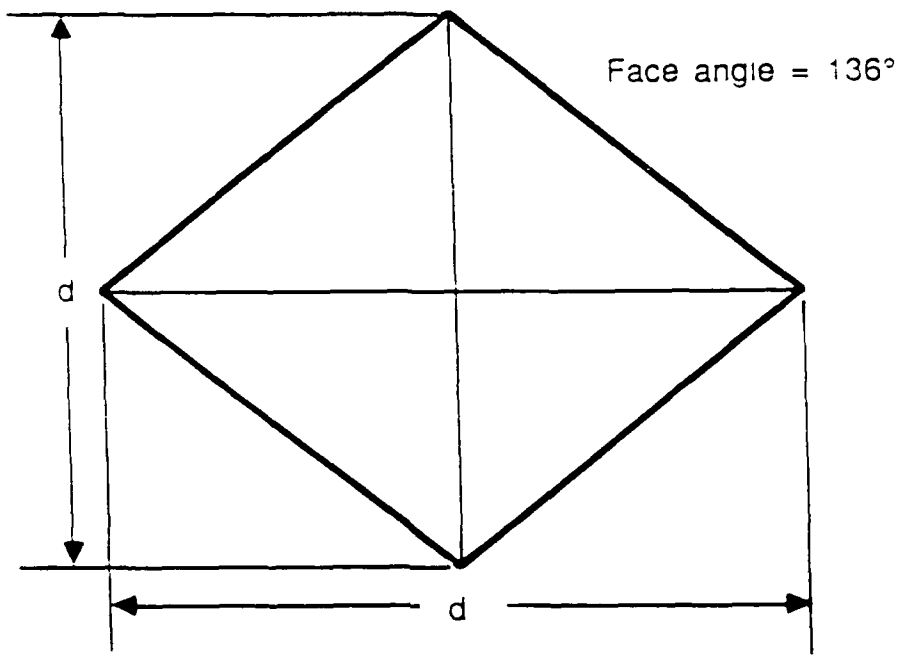

Figure 21. Two-dimensional model for Vicker's micro-hardness indentation.

$$HV = \frac{2\,F \sin\frac{136^\circ}{2}}{d^2} = 1.854\,\frac{F}{d^2} \qquad (7)$$

Where F is in kilograms force (Kg_f) and d is in mm. The units of HV will be Kg_f/mm^2.

The indentations were located such that they did not contact any fibers that were present in the cross-section. A load of 0.294 N (0.030 kg_f) was used. Smaller loads than this produced indentations too small to be accurately measured. The load was kept on the indenter for approximately 30 seconds after the indenter contacted the test specimen. Prior to the microhardness tests, test specimens were saw cut and cold mounted in plastic. The specimens were polished using very fine abrasive paper with a final cloth polishing with 10 micron alumina suspended in distilled water. The resulting finish was suitable for light microscope examination.

4.3 Procedures for Microscopic Examination

Microscopic examinations were carried out by optical microscopy and scanning electron microscopy (SEM). Specimens similar to those described in section 4.2 were used for examination by optical microscopy. The specimens were examined for fiber distribution, metal infiltration and the fiber/matrix interface. The polished specimens were etched with a warm dilute NaOH solution. Cross-sections cut parallel to and those perpendicular to the fibers were examined.

A scanning electron microscope was used to examine the fracture surface of the castings fractured under tensile loading. In

addition, fibers at different stages of the processing were examined. Fibers prior to casting, after casting and after heat treatment at temperatures slightly greater than the solidus temperature were examined. The fibers were extracted from the matrix of the castings by dissolving the matrix in concentrated warm NaOH.

4.4 Damping Measurement

Cantilevered beams were used for the damping measurements. The beams were clamped on one end and vibrated on the other in the thicker dimension of the cross-section. The details of the experimental configuration are shown in Figure 22. The sinusoidal frequency is produced by a frequency generator and monitored by a frequency counter. The signal is amplified and sent to a switching box where it is split and sent to an oscilloscope and a copper coil which, in turn, produces a varying electromagnetic force on a small cobalt-samarium magnet attached to the lower tip of the specimen as shown in Figure 22. A small piece of aluminum foil is attached to the upper tip of the beam in order to provide a reflecting surface for the probe of the photoaccumulator device. The photoaccumulator provides information on the displacement of the beam as it vibrates by sending and receiving an optical signal through a fiber optic system. The vibration amplitude signal is sent to a signal band-pass filter which allows only a narrow range of frequencies around the natural frequency of the beam to pass through. The filtered signal is further sent to an oscilloscope where it is monitored and an accurate value for the natural frequency is determined. At this natural frequency, the current to the coil is cut-off simultaneously

triggering the storage oscilloscope which records the pattern of the vibration decay. A photograph is taken of the vibration decay and logarithmic decrement (δ) is calculated using the following relationship:

$$\delta = \frac{1}{n} \ln \left(\frac{x_0}{x_n}\right) \tag{8}$$

Where x_0 is equal to the initial amplitude and x_n is equal to the amplitude after n cycles.

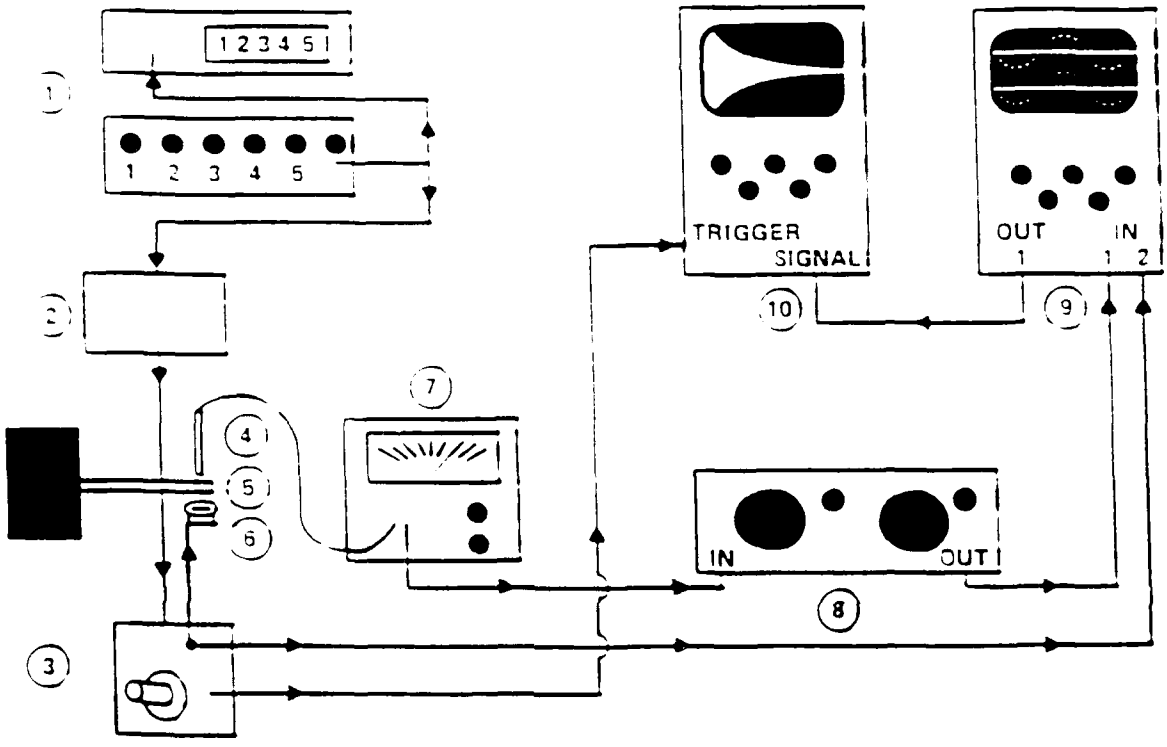

Figure 22. Experimental set-up for damping measurements on clamped-free cantilevered beam specimens [28]: (1) signal generator and counter, (2) amplifier, (3) switching box, (4) probe of photoaccumulator device, (5) specimen, (6) coil, (7) photoaccumulator device, (8) frequency filter, (9) monitor oscilloscope and (10) storage oscilloscope.

Chapter 5

RESULTS AND DISCUSSION

The purpose of the testing and characterization procedures described in the previous chapter was to provide insight into the physical and mechanical properties of the fiber reinforced castings fabricated using high pressure squeeze casting. In particular, it was desired to know which properties are effected by the process and how. For example, did the process damage or degrade the fibers? And what was the extent of the chemical reaction between the fibers and the aluminum alloy? Also, what was the effect of the process on the properties of the matrix? To answer these questions and to address related issues, the results are presented and discussed in this chapter.

5.1 Physical Examination of Squeeze Cast Fiber Reinforced Aluminum

The castings produced using the procedures described in Chapter 2 are generally 70 mm (2.7 inch) in diameter and had an average thickness of 3.2 mm (0.125 inch). The two types of reinforcement, planar random and unidirectional, can be easily distinguished with the parallel fiber tows being easily visible of the surface on the unidirectionally reinforced castings. The overall surface characteristics of both types of castings are very good with

the notable absence of any shrinkage or other typical casting defects.

Figure 23 shows the fiber distribution in the planar random and unidirectional fiber reinforced castings. There was good overall distribution of the fibers throughout the cross-section of the casting. The distribution of the planar random fibers was particularly uniform while the fiber tows in the unidirectional reinforced casting were slightly concentrated toward the top and bottom of the casting. This was due to the nature of the packing of the fiber tows and the relative difficulty in infiltrating this arrangement as the aluminum flowed from the center to the top and bottom of the casting.

The degree of metal infiltration in the fiber tows of the unidirectionally reinforced castings can be seen in Figure 24. The aluminum alloy completely surrounded each individual filament of the tow. It should also be noted from this figure that there are a significant number of the fibers from the planar random fiber sheets that are oriented parallel to the tow fibers. This qualitatively supports the inclusion of these fibers in the generation of Figure 9 in Chapter 2.

A polished cross-section of a casting oriented parallel to the principal fiber direction in the unidirectionally reinforced casting is shown in Figure 25. Several breaks in the fibers can be seen. The presence of metal between the separated ends indicates that the fibers were broken during initial infiltration by the liquid aluminum. This situation is typical with nearly all the fibers showing some degree of breakage at some point along its length in the casting.

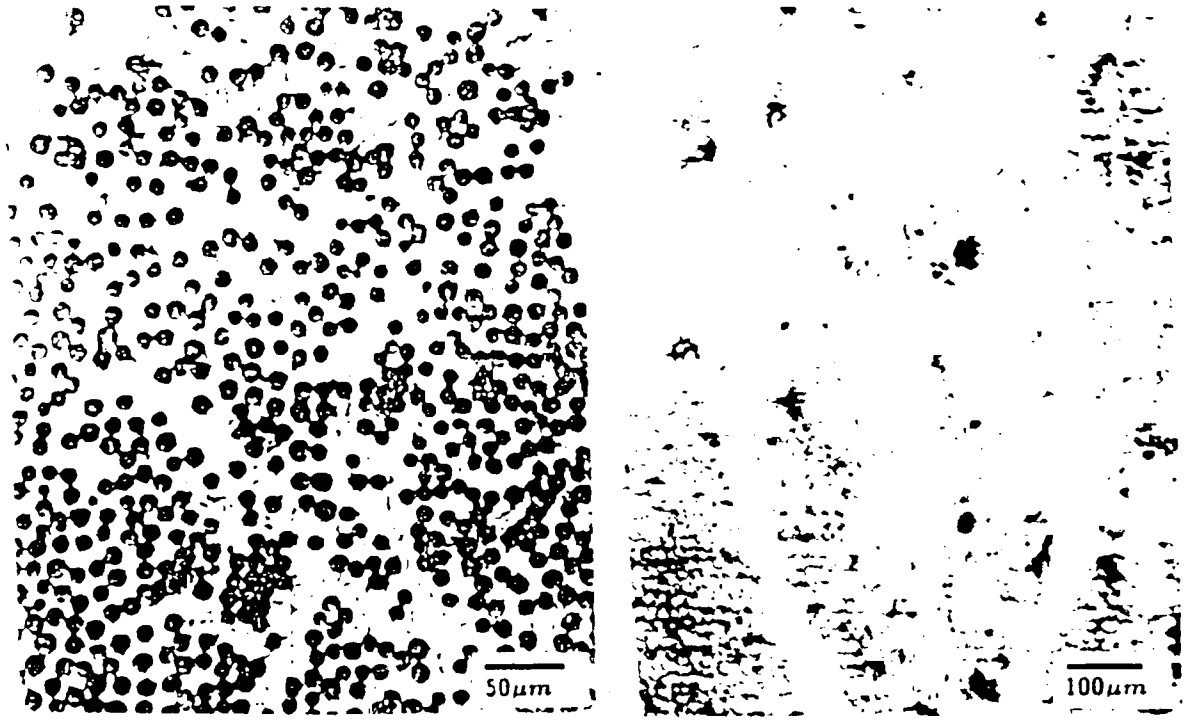

Figure 23. Light micrographs showing fiber distribution in graphite fiber reinforced castings: a) planar randomly oriented fiber reinforced casting and b) unidirectional fiber reinforced casting.

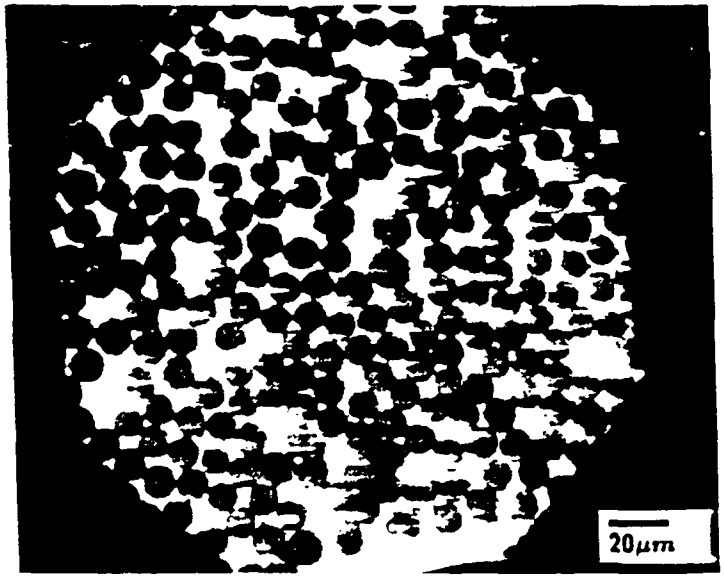

Figure 24. Light micrograph showing degree of metal infiltration into unidirectional fiber tow

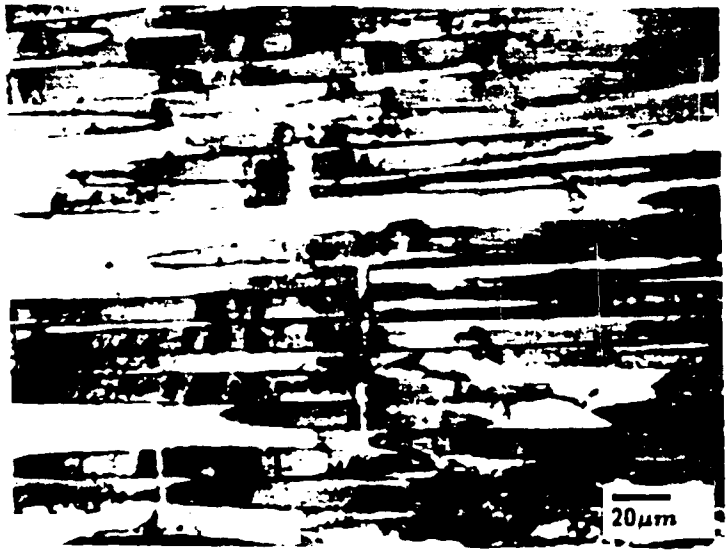

Figure 25. Light micrograph of cross-section from unidirectional fiber reinforced casting showing breaks in the length of the fibers

Although the fibers are no longer continuous from one end of the casting to the other, the average length of the fibers is still much greater than the critical fiber length that is necessary for the fiber to theoretically achieve its maximum allowable stress. The critical fiber length is on the order of 0.3 mm (0.012 inch) while even the smallest fiber segments observed were well over a magnitude larger than this critical value. The as-cast fiber lengths were determined by examining fibers on polished cross-sections and fibers exposed by dissolving the aluminum matrix with NaOH.

In order to observe the extent of reaction between the fiber and the aluminum alloy matrix, polished cross-sections were etched with NaOH and examined by light microscopy. A micrograph of a casting is shown in Figure 26 a. There is no observable reaction zone even after etching. A micrograph of a casting which was heat treated at 823 K (1022 °F) for 100 hrs is shown in Figure 26 b. In this case, there was some observed reaction zone around the fibers on the etched cross-section. After heat treatment above the solidus temperature of the aluminum alloy there was a readily apparent reaction zone. This is illustrated in Figure 26 c. By comparing these three micrographs, it can be seen that there had been relatively little reaction in the as-cast condition and that it is necessary to heat the casting above the solidus temperature of the matrix in order to effect any appreciable reaction.

Another method that was used to determine the extent of reaction between the graphite fibers and the aluminum alloy was to expose the fibers by dissolving the aluminum matrix with NaOH and examine the fibers using scanning electron microscopy. A SEM

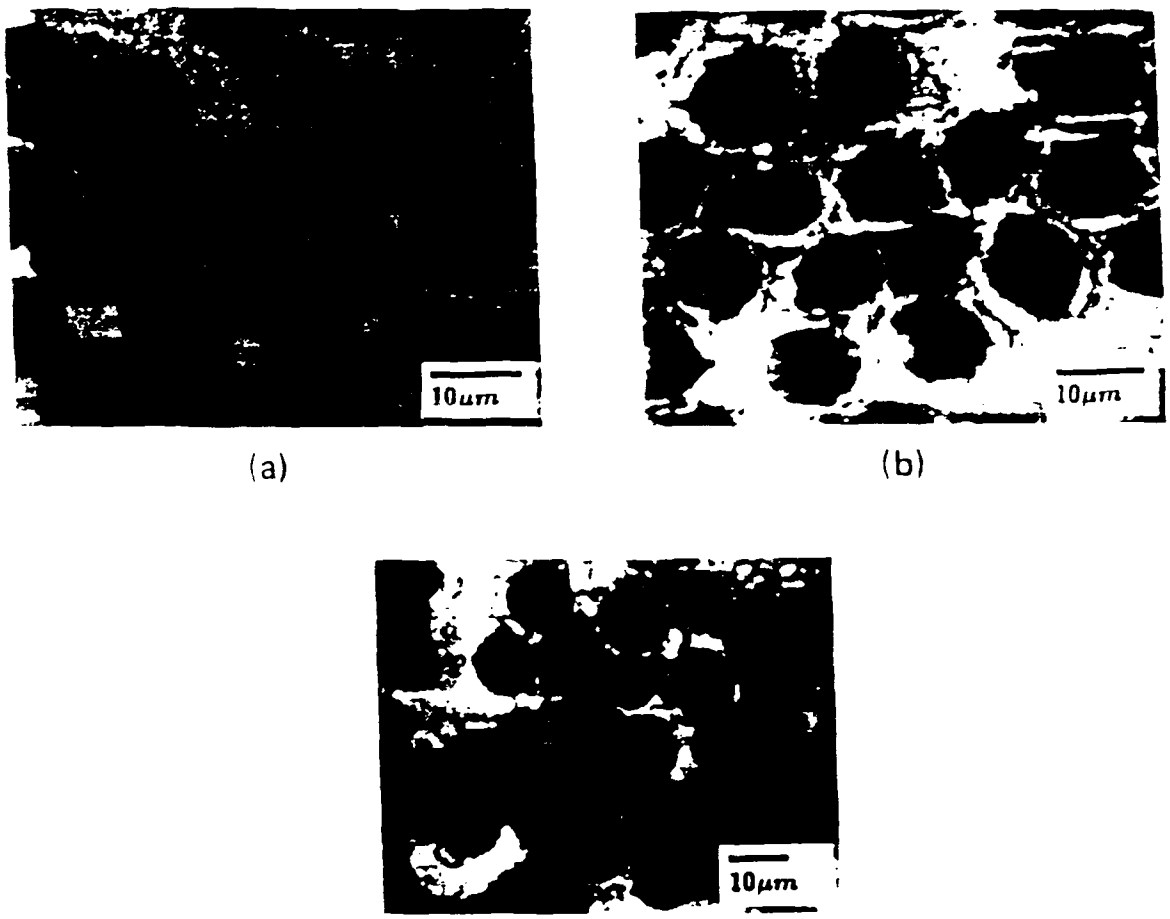

Figure 26. Micrographs of polished and etched cross-sections showing presence of reaction zone around fibers: a) as-cast, b) after high temperature heat treatment and c) after heat treatment at temperature above solidus temperature for 6061 aluminum.

micrograph of a fiber before casting is shown in Figure 27 a. SEM micrographs of fibers in the as-cast condition and after very high temperature (above the solidus temperature) heat treatment are shown in Figures 27 b and c, respectively. Here the reaction products appear as thin crystals oriented perpendicular to the fiber axis. Again it can be seen that although there is some limited reaction evident in the as-cast condition, there is significant reaction after the very high temperature heat treatment. Similar reaction products were identified by Kohara and Muto [20]. As an illustration one of the fibers from their investigation is shown in Figure 28. In their investigation, the fibers were exposed to molten aluminum for various times and the extent of degradation in the tensile strength of the fibers was determined. For the fiber shown, the exposure time was around 2 minutes. Thus, our finding of reaction products at the fiber/matrix interface is consistent with published work. Kohara and Muto [20] suggested that the reaction product was Al_4C_3.

5.2 Mechanical Property Characterization of Fiber Reinforced Castings

This section will describe the tensile properties of the fabricated graphite fiber reinforced castings. Although the focus was on unidirectional fiber reinforcement the data from the tests on castings with planar random reinforcement will also be discussed for comparison. The tensile strength of the castings will be discussed first followed by a discussion of the stiffness and the fracture strain. Scanning electron micrographs of the fracture

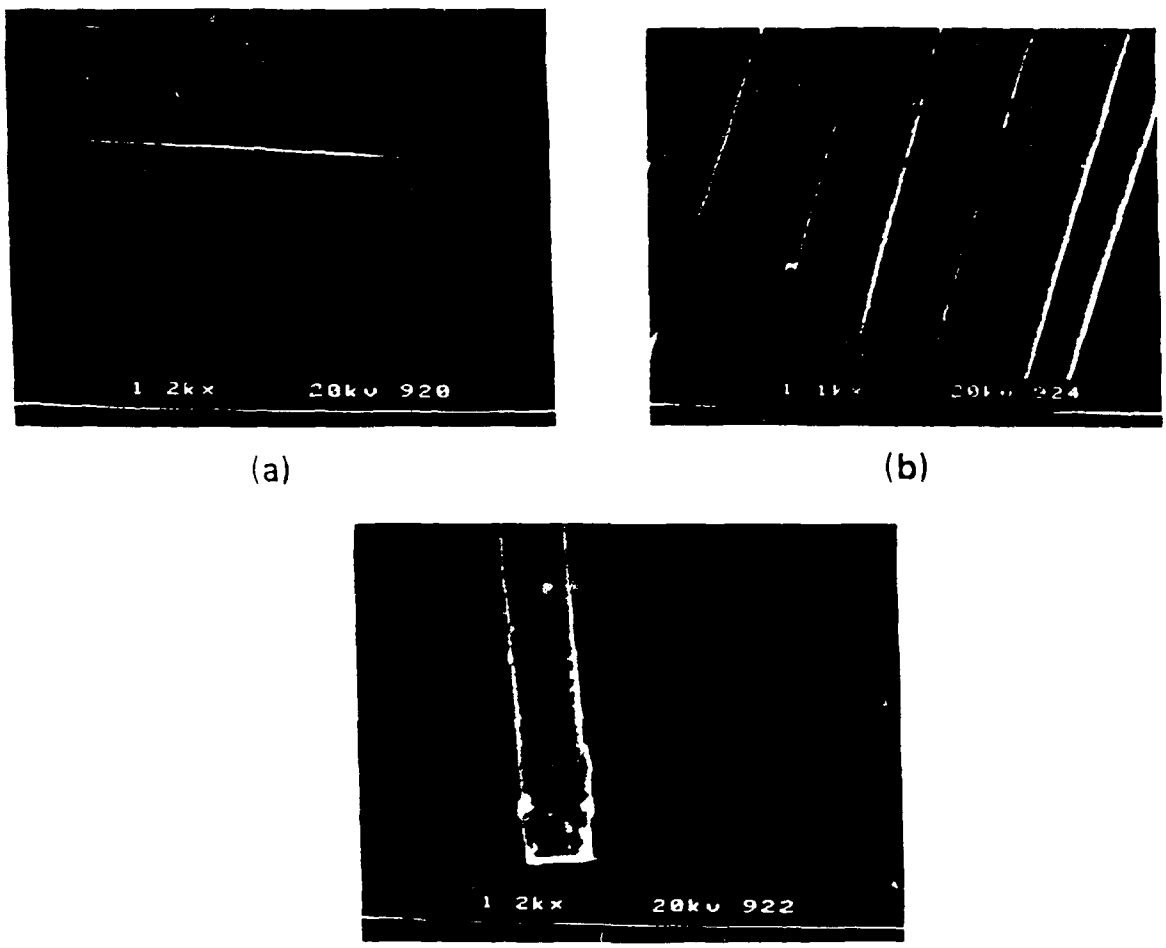

Figure 27. SEM micrograph of fibers exposed by dissolving matrix: a) before casting, b) after casting and c) after heat treatment at temperature above solidus temperature for 6061 aluminum.

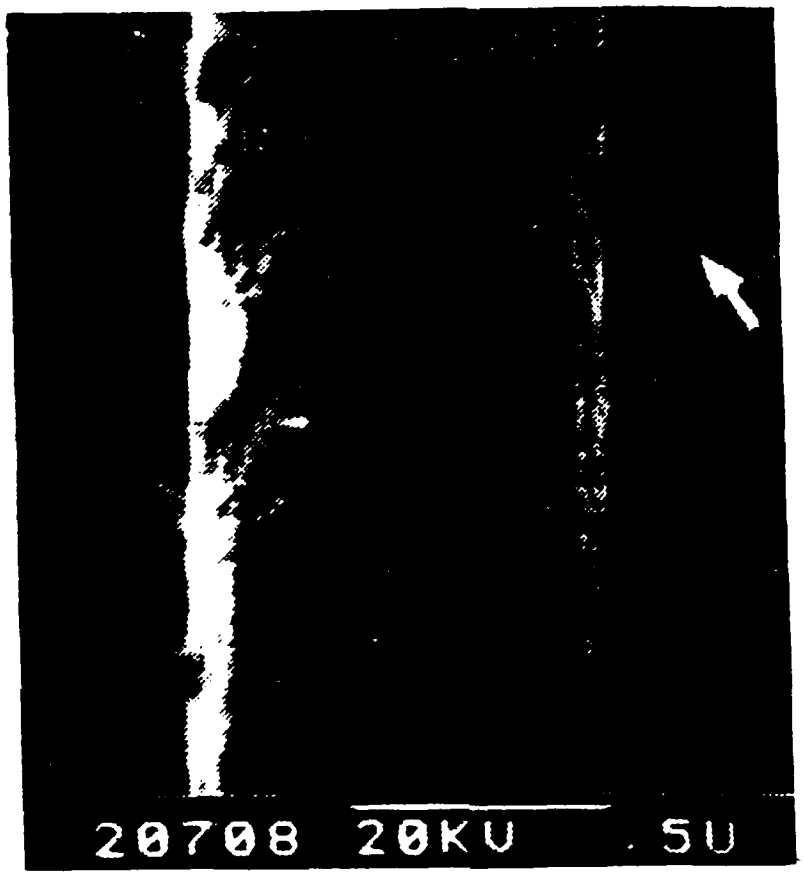

Figure 28. Carbon fiber from investigation by Kohara and Muto [20] showing reaction products on fiber surface after exposure to molten aluminum for approximately 2 minutes

surfaces will also be presented. In the last part of this section, a model will be proposed to explain the tensile behavior of the as-cast reinforced castings.

5.2.1 Tensile Strength and Fracture Strain

The tensile strength of the planar random carbon fiber reinforced reinforced aluminum castings as a function of fiber volume fraction is shown in Figure 29. There exists a peak in the strength which is equal to 320 MPa (46 ksi) and it corresponds to a fiber volume fraction of around 30 percent. This peak may be explained by the presence of the off-axis fibers in the casting. At higher volume fractions, there are more of these fibers and less matrix. These fibers begin to act as defects causing failure at lower and lower loads. The failure at the low loads may ultimately be explained by a complex stress distribution in the area of fiber intersections where the amount of matrix may be very small. Some fibers may even be touching each other.

The strength of the matrix, squeeze cast with no fiber reinforcement, was measured to be 179 MPa (26 ksi). This represents a significant improvement over the strength of 6061-O Al which is approximately 124 MPa (18 ksi) [23]. The unidirectional fiber reinforced castings were fabricated with fiber volume fractions ranging from 4 percent to 52 percent. The tensile strength of the unidirectional fiber reinforced castings as a function of fiber volume fraction is given in Figure 30. Over the entire range of fiber volume fractions investigated, the tensile strength of the reinforced castings increased with increasing fiber volume fraction.

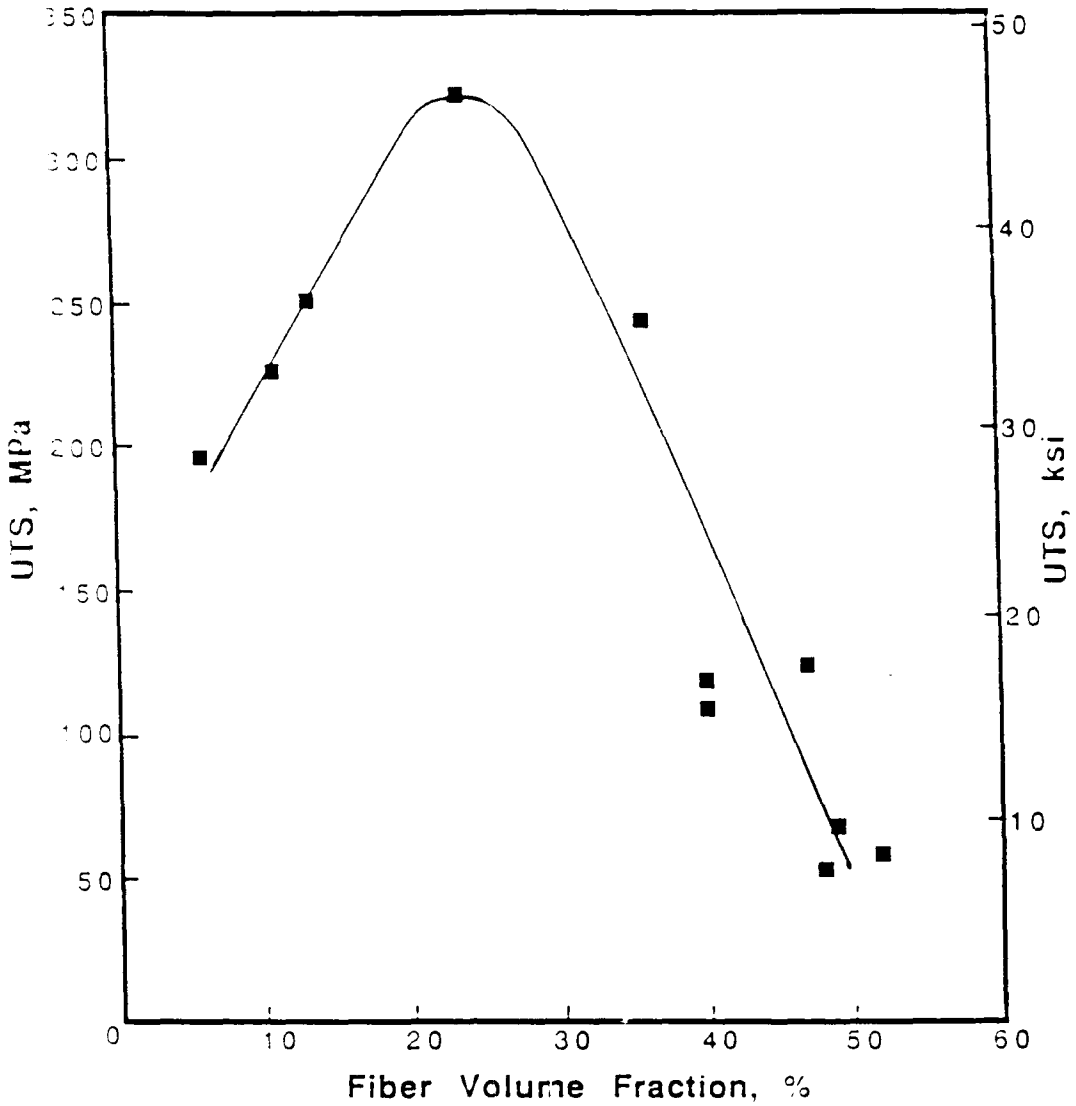

Figure 29. UTS of planar randomly oriented graphite fiber reinforced aluminum castings fabricated by high pressure squeeze casting as a function of fiber volume fraction

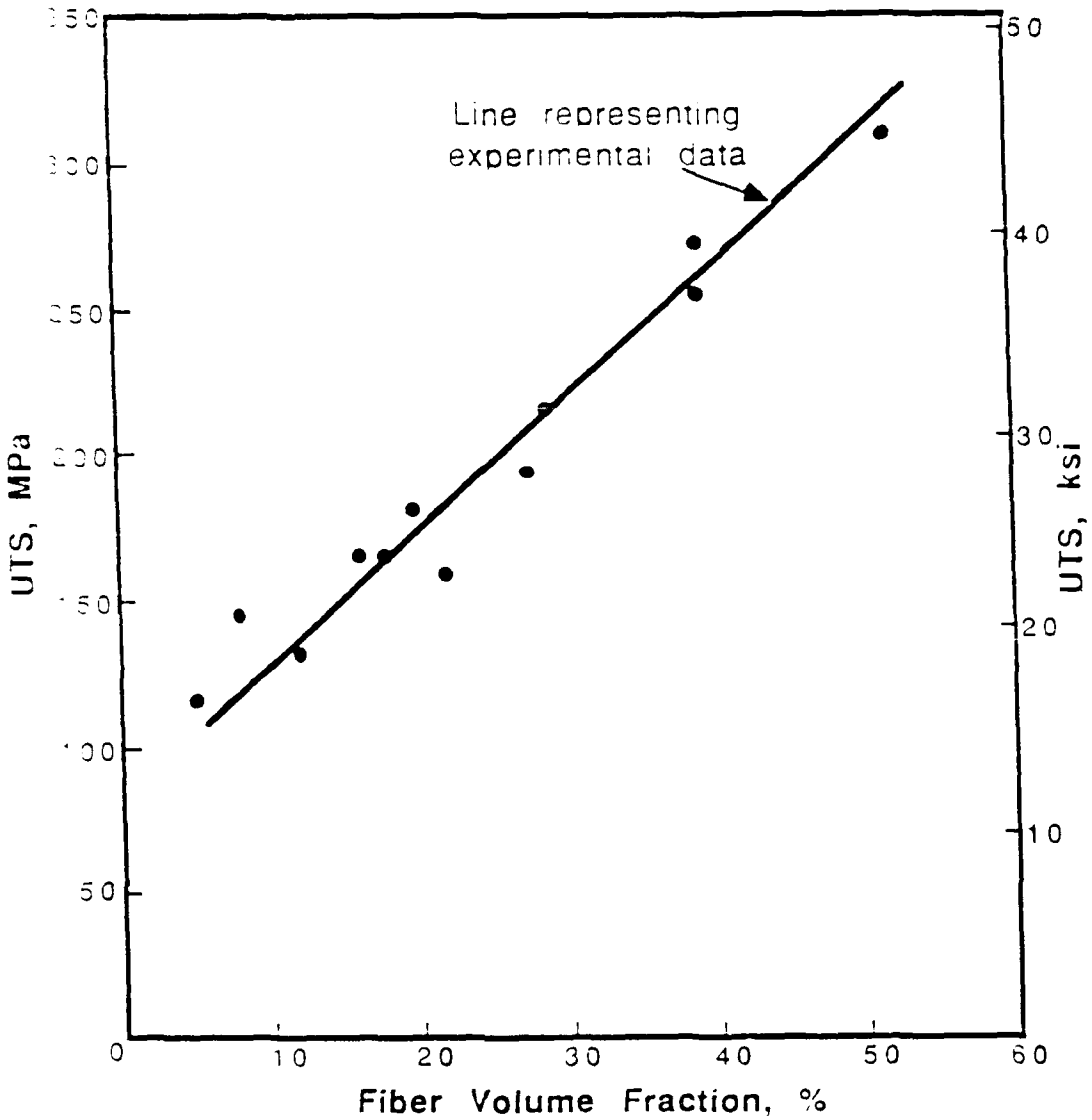

Figure 30. UTS of unidirectional graphite fiber reinforced aluminum castings fabricated by high pressure squeeze casting as a function of fiber volume fraction

Although a direct quantitative comparison of the strengths of the two types of fabricated reinforced castings (planar random and unidirectional) is not possible because the mechanical properties of the planar random fibers differ significantly from those of the P-55 tow fibers (refer to Table 2), the strength data seem to suggest some interesting things to consider. For example, a design may require equal material strength and stiffness in several different directions in the same plane. For this case, a planar random fiber reinforced metal would be an ideal choice considering its isotropic behavior in the fiber plane. If planar random fiber reinforced metal is used, however, the designer should be cautious not to specify a fiber volume fraction above that which corresponds to the peak strength. If the strength requirements of the design exceed this maximum value, then a laminate design involving unidirectional reinforcement would need to be considered.

Examination of the fracture surfaces using scanning electron microscopy showed a very high degree of fiber pull-out for the unidirectional graphite fiber reinforced aluminum alloy. Fiber pull-out can be distinguished from de-bonding by the clean appearance of the fiber surface as seen in Figure 31. If there is a strong bond or diffusion bond between the fiber and the matrix, then upon failure and subsequent withdrawal of the fiber from the matrix, the fiber surface will show a significant amount of matrix and reaction products still adhering to the fiber. The absence of these features, suggest that the principal type of bonding between the fiber and the matrix in the squeeze cast metals is adhesion type where the load is transferred by the matrix to the fibers through a friction force at

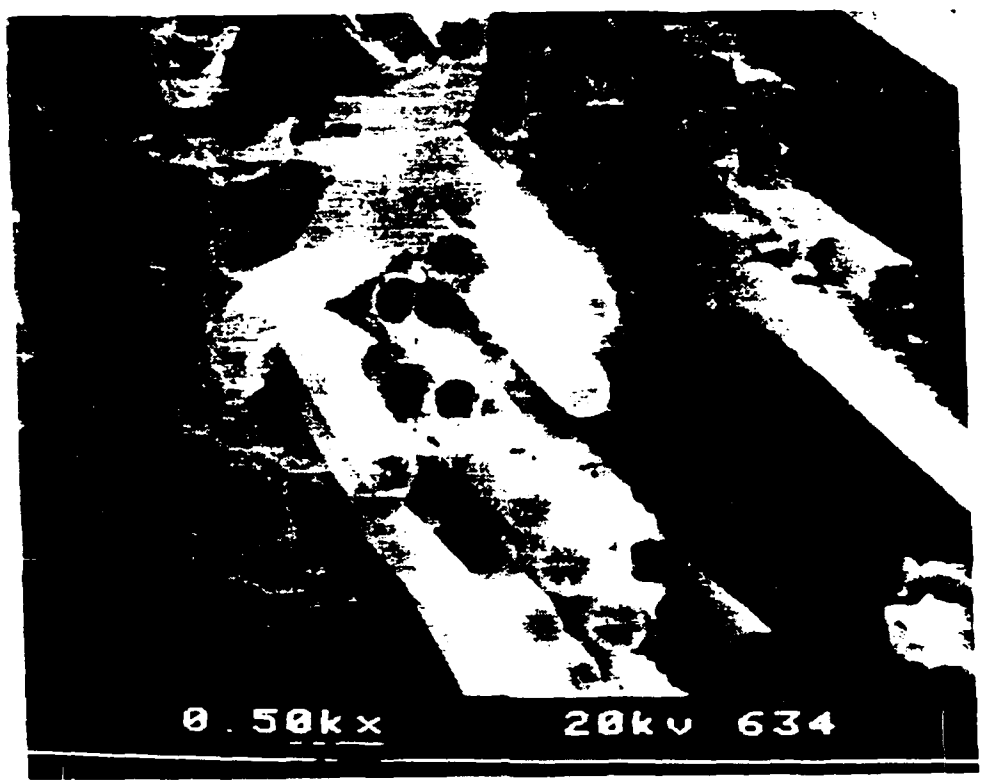

Figure 31. SEM micrograph of graphite fiber on tensile fracture surface. Fiber pull-out holes are also visible on the fracture surface.

the fiber/matrix interface. The pull-out holes are also visible on the fracture surface in the background where the corresponding fibers would be on the opposite fracture surface. Similar observations were made for planar random graphite fiber reinforced castings, as well.

The fracture strain of the reinforced unidirectional Gr/Al castings was determined by using a strain gage and recording the strain at failure. The typical fracture strain for the unidirectional Gr/Al castings was 0.49 percent, which is significantly lower than the expected fracture strain of the fiber (0.60 percent) and well below the fracture strain of aluminum. The fact that the castings failed at a strain lower than the fracture strain of the fibers is an indication that the mechanical behavior of the squeeze cast fiber reinforced aluminum alloy is complex and requires an in-depth analysis. An attempt has been made to explain the observed tensile strength and fracture strain behavior of the fabricated materials in the following section.

5.2.2 Tensile Strength Model

This section describes a model proposed to explain the tensile behavior of the unidirectional graphite fiber reinforced aluminum fabricated in this study. Although the tensile strength of the castings increased with increasing fiber volume fraction, a simple rule of mixtures model does not accurately describe the behavior. For example, the rule of mixtures strength for unidirectional continuous graphite fiber reinforced aluminum with a fiber volume fraction of 0.30 is approximately 715 MPa (104 ksi) while the

experimental value was 207 MPa (30 ksi). There are a number of the reasons why the strength of the as-cast reinforced castings were so significantly lower than the predictions by rule of mixtures. In particular, the fibers could have been degraded by chemical reaction with the molten aluminum. It was already established, however, that there was only very limited reaction between the fibers and the matrix in the as-cast condition. In that case, there may have been too little reaction.

Even if there were no reaction, in which case the matrix would contribute nothing to the strength of the casting, the strength should still be given by

$$\sigma_c = \sigma_f V_f \qquad (9)$$

Where σ_f is the strength of the the fibers. In this case, the predicted strength of the casting (fibers) with fiber volume fraction equal to 30 percent is 641 MPa (93 ksi), still significantly greater than the experimental value of around 200 MPa (30 ksi).

Another possibility is that the fibers were crushed during casting and the average length is less thar the critical fiber length for an aligned discontinuous graphite fiber reinforced aluminum. It has already been shown, however, that the average fiber length in the casting was much greater than the critical fiber length.

In the model proposed the fibers are broken at random position along the gage length of the specimens used for tensile testing and there is not sufficient bonding between the aluminum and the graphite in order to stress the fibers to failure. Therefore, during

testing, the ends of the fibers in the gage section of the specimen are pulled from the aluminum when the interfacial bond between the graphite fibers and the aluminum is broken. There are two basic assumptions in this statement that represent the basis for the model described below: the fibers are long but not continuous and the fibers are pulled from the matrix rather than being broken.

The model is first described in terms of the behavior of a single fiber. The single fiber model is illustrated in Figure 32. From equilibrium of forces we can write

$$P_{fs} = \tau (2\pi rL) \qquad (10)$$

Where : P_{fs} = the load on the fiber

τ = the shear stress at the fiber/metal interface

r = the radius of the fiber

L = the length of the fiber embedded in the metal

However, Equation 10 has a limit value where the fiber will no longer be pulled from the matrix but will break instead. This value is given in Equation 11.

$$(P_{fs})_{max} = \sigma_{fu} (\pi r^2) \qquad (11)$$

Where : σ_{fu} = the ultimate tensile strength of the fiber

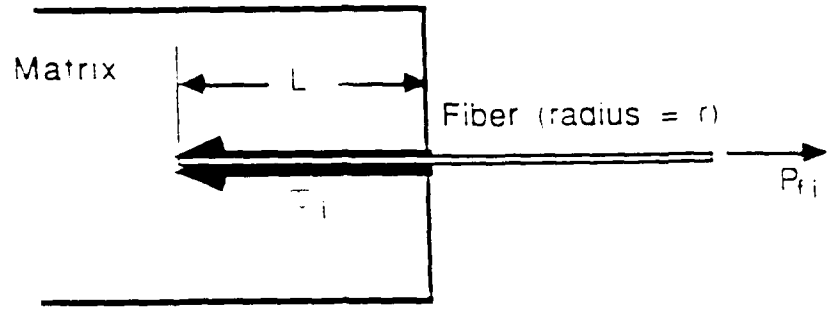

Figure 32. Single fiber model for fiber embedded in a metal matrix

Combining Equations 10 and 11, a minimum interface shear strength can be defined as that which is necessary for the fiber to be broken rather than pull-out. This relation is given as Equation 12.

$$(\tau_i)_{min} = \frac{\sigma_{fu} r}{2L} \qquad (12)$$

The load on the overall fiber reinforced metal, P_c, is equal to the sum of the loads on the fibers and on the metal or

$$P_c = P_f + P_m \qquad (13)$$

Where: P_f = the load on the fibers
P_m = the load on the matrix

Considering all the fibers, Equation 9 can be written as

$$P_f = N (2\pi rL) \tau_i \qquad (14)$$

The load on the matrix can also be expressed simply as

$$P_m = \sigma_m A_m \qquad (15)$$

Where: Am = the fractional area occupied by the matrix

From Rule of Mixtures we know:

$$\sigma_c = \sigma_f V_f + \sigma_m (1-V_f) \qquad (16.a)$$

And from Equation 12 it can be shown that

$$\sigma_f = (2\frac{L}{r}\tau_i) \qquad (16.b)$$

Substituting Equation 16.b into 16.a yields

$$\sigma_c = (2\frac{L}{r}\tau_i) V_f + \sigma_m (1-V_f) \qquad (16.c)$$

The ultimate strength of a fiber reinforced material described by this model can be obtained from Equation 16.c and is given by

$$\sigma_{ult} = (2\frac{L}{r}\tau_{iu}) V_f + \sigma_m^* (1-V_f) \qquad (17)$$

Where σ_m^* is the stress on the metal at the overall strain when the interface fails or the pull out starts and may be evaluated by determining the intercept of the experimental line in Figure 30. Rearranging Equation 17, we can write

$$\tau_{iu}(\frac{L}{r}) = \frac{\sigma_{cu} - \sigma_m^* (1-V_f)}{2 V_f} \qquad (18)$$

Equation 18 can now be used to determine the experimental value for the product of the interfacial shear strength and the fiber aspect ratio (L/r). This value should be constant since it represents

the line described by the relation between τ_u and V_f. But as it can be seen there is some scatter in the experimental data in Figure 30 that result in slightly different values for the product at different fiber volume fractions. These values are listed in Table 13 as a function of fiber volume fraction. The average experimental value for the product of the interfacial shear stress and the aspect ratio was 266 MPa (38.6 ksi) with some scatter ranging from 214 MPa (31.0 ksi) to 298 MPa (42.7 ksi).

The next step is to compare the experimentally determined value of the product with the minimum value that would be required to break the fibers. Again rewriting Equation 12 we have:

$$\tau_{i\,min}\left(\frac{L}{r}\right) = \frac{\sigma_{fu}}{2} = 1050 \text{ MPa} \quad (152 \text{ ksi}) \qquad (19)$$

For our castings we can assume the the fiber aspect ratio is a constant; evaluating Equation 19 then yields a minimum value for the interfacial shear strength as a function of the fiber aspect ratio of 1050 MPa (152 ksi) when the ultimate tensile strength of the fibers equals 2100 MPa (304 ksi). It can be seen that the average experimental shear strength is only about 25% of the value predicted in Equation 19 or 272 MPa (40 ksi). Now we can explain why the strength of the fabricated Gr/Al castings was only about 25-30% of the rule of mixtures predictions, i.e. the bond was only 25 percent as strong as it should have been to develop the maximum stress in the fibers. It also indicates that by improving the interfacial bond the strength of the as-cast unidirectional reinforced aluminum can be

Table 13. Experimental values for product of interfacial shear strength and the fiber aspect ratio as a function of fiber volume fraction

V_f	σ_{cu}, MPa (ksi)	$\tau_{iu}(\frac{L}{r})$, MPa (ksi)
0.16	165 (24)	298 (43)
0.18	165 (24)	269 (39)
0.20	179 (26)	281 (41)
0.22	159 (23)	214 (31)
0.28	193 (28)	238 (35)
0.29	214 (31)	267 (39)
0.38	276 (40)	295 (43)
0.38	255 (37)	268 (39)
0.52	310 (45)	260 (38)
		Ave. = 266 (39)

ncreased further. The the proposed pull-out model represented by Equation 17 adequately explains the experimental results for the strength of the unidirectional reinforced castings.

5.3 Stiffness

A typical load versus displacement curve for a unidirectional graphite fiber reinforced casting is shown in Figure 33. The curve can be approximated by two straight lines with different slopes. The first being the primary or elastic modulus for the casting and the second being the secondary modulus. Since the graphite fibers are essentially perfectly elastic the elastic-plastic behavior of the castings can be attributed to the elastic-plastic behavior of the matrix. From strain gage measurements, stiffnesses of castings with fiber volume fractions of 20 percent and 50 percent were 100 GPa (14.5 Msi) and 150 GPa (21.8 Msi) , respectively. These values are lower than the rule of mixtures values of 131 GPa (19.0 Msi) and 224 GPa (32.5 Msi), respectively. The relatively lower values of stiffness for the Gr/Al castings needs further investigation.

The following section of this chapter describes the effects of the squeeze casting process and the heat treatment on the properties of the 6061 aluminum by conducting microhardness measurements.

5.4 Microhardness of Squeeze Cast Aluminum

By characterizing the microhardness of the squeeze cast aluminum at different stage during the squeeze casting and heat

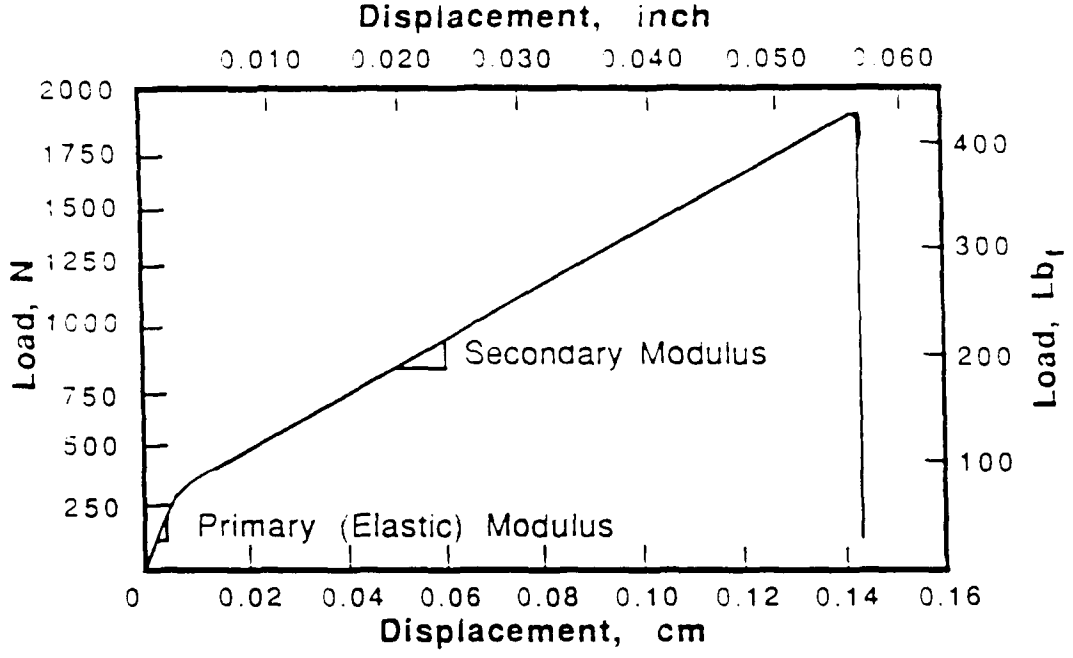

Figure 33. Typical load vs. displacement curve for unidirectional graphite fiber reinforced aluminum castings fabricated by high pressure squeeze casting.

treating processes insight can be gained into the effect of these processes on the microstructure.

The microhardness data obtained for the 6061 aluminum at different conditions is given in Table 14. A standard 6061-T6 aluminum specimen was prepared and the experimental average was 101.3 (in the customary units of kg_f/mm^2). This value is in good agreement with literature the value for this material of around 102 [23].

The average value for the squeeze cast aluminum with no fiber reinforcement was 74.1 which is significantly higher than the 6061-O aluminum alloy which is 31.4 [23]. This improvement is probably due to an effective heat treatment of the 6061 aluminum alloy just after it solidifies during casting. At that time the temperature will still be very high and there should be a considerable number of vacancies caused by the pressure causing very rapid cooling. Both of these factors can combine to result in rapid precipitation hardening of the alloy [29].

With fiber reinforcement the hardness of the aluminum in the as-cast condition fell to 53.6 while this value is less than the un-reinforced squeeze cast aluminum, presumably caused by interference of the fibers to precipitation, it is still considerably higher than that of 6061-O aluminum and is approximately equal to the hardness for 6061-T4 Al which is 56.8 [23]. When heat treated the hardness of the matrix falls still further to around 39.5, close to the hardness of 6061-O Al. This was probably due to over-aging of the matrix alloy.

Table 14. Experimental Vickers microhardness data

Test Specimen (Condition)	Test load (kg)	Ave. Diagonal (mm)	HV (kg/mm²)
6061-T6 Al	0.030	0.0235	99.7
		0.0240	95.6
		0.0229	105.0
		0.0229	105.0
		Ave. =	101.3
6061 Al (Squeeze cast w/ no fibers)	0.030 (Tested near middle of casting)	0.0272	75.2
		0.0275	73.5
		0.0280	70.9
		0.0250	89.0
		0.0248	90.4
		Ave. =	79.8
6061 Al (Squeeze cast w/ no fibers)	0.030 (Tested near the edge of casting)	0.0278	72.0
		0.0290	66.1
		0.0285	68.5
		0.0300	61.8
		0.0280	70.9
		0.0280	70.9
		Ave. =	68.4
6061-Al (Squeeze cast. V_f = 0.15)	0.030	0.0335	49.1
		0.0320	53.8
		0.0322	53.1
		0.0305	59.2
		0.0320	53.8
		0.0340	47.6
		0.0322	53.1
		0.0305	59.2
		Ave. =	53.6

Table 14. Continued)

Test Specimen (Condition)	Test load (kg)	Ave. Diagonal (mm)	HV (kg/mm²)
6061-Al (Heat teated 873 K for 100 Hr.)	0.030	0.0354	44.4
		0.0358	43.4
		0.0373	40.0
		0.0358	43.4
		0.0360	42.9
		0.0369	40.8
		Ave. =	42.5
6061-Al (Heat treated above solidus temperature of Al)	0.030	0.0384	37.7
		0.0385	37.5
		0.0403	34.2
		0.0395	35.6
		0.0440	28.7
		0.0405	33.9
		0.0383	37.9
		0.0359	43.2
		0.0375	39.6
		Ave. =	36.5

5.5 Damping

The results of the analysis of the damping of the unidirectional graphite fiber reinforced aluminum castings fabricated in this study are shown in Table 15. Although the values vary slightly with fiber volume fraction, there does not seem to be a strong correlation indicated by the experimental data. However, comparison of the overall averages of the logarithmic decrement (ignoring any effects of fiber volume fraction) suggest that, in general, the damping in the 90° beams is higher, up to 2 times higher, than the damping in the 0° beams. For mode I vibration, the damping in the 90° direction is 1.6 times higher than in the 0° direction, neglecting the extreme value of 18.0 for 0°, V_f = 28.9. The 90° damping for modes II and III are also higher than the corresponding 0° damping, 2.3 and 1.1 times higher, respectively. These results are as expected as the stiffnesses of the unidirectional beams are much higher in the fiber (0°) direction than in the transverse direction.

5.6 Finite Element Analysis of Transient Thermal Behavior of Squeeze Casting Process

The transient thermal behavior of the squeeze casting process was modelled as described in Chapter 3. The method involved the use of a finite element program called THERM that was modified to have the capability for axisymmetric elements. The program was tested by first solving two test problems before attempting to model the thermal behavior of the high pressure squeeze casting process.

Table 15. Logarithmic decrement values for unidirectional Gr/Al fiber reinforced beams†

	Logarithmic Decrement (x 10^{-3})					
v_f	Mode I		Mode II		Mode III	
%	0°	90°	0°	90°	0°	90°
18.9		3.9		11.2		
21.1	7.8		2.1			
23.3		10.2		6.0		4.7
24.4		7.7				
25.6		3.6		6.2		
26.7		3.2		6.9		5.2
27.8		12.4		6.9		
28.9	18.0		3.5	3.9		
31.1	4.7		2.9			
32.2	4.9		3.5		5.8	
33.3	6.6		2.6		3.2	
Overall Average	6.0*	9.7	2.9	6.8	4.5	5.0

† 0° refers to fiber reinforcement parallel to beam length. 90° refers to reinforcement parallel to the thicker dimension of the cross-section of the beam.

* Neglecting relative extreme value of 18.0 at v_f = 28.9

5.6.1 Test Problems

The results of the one-dimensional test problem are given in Figure 34. The line in Figure 34 represent the predicted location of the solidification front as a function of time. Superimposed on this line are points that represent the exact solution at the corresponding times as obtained from the literature [27]. There was very good agreement between the predicted location and the literature values.

The results from the two-dimensional test problem are given in Figure 35. The line in Figure 35 represents the solidification front at a time equal to 1 second as predicted by THERM. Again the points represent the literature solution that was obtained using a finite difference method. As in the one-dimensional problem, there was good agreement between the predicted location obtained using THERM and that obtained from the literature.

5.6.2 Results from Experimental Model

The results from the experimental model are given in Figure 36. The first step in the three step model, as described in Chapter 3, was used for times from 0 to 1.5 seconds, the second condition was used for times ranging 1.6 to 3.0 seconds and the third condition was used for times from 3.1 seconds to 4 seconds. In the time frame from 3 to 4 seconds, the aluminum cooled very rapidly as it infiltrated the fibers and came into contact with the die wall. The slowing of this rapid decrease in temperature is attributed to the aluminum solidifying. After four seconds the average temperature of the aluminum had fallen to just below the solidus temperature of

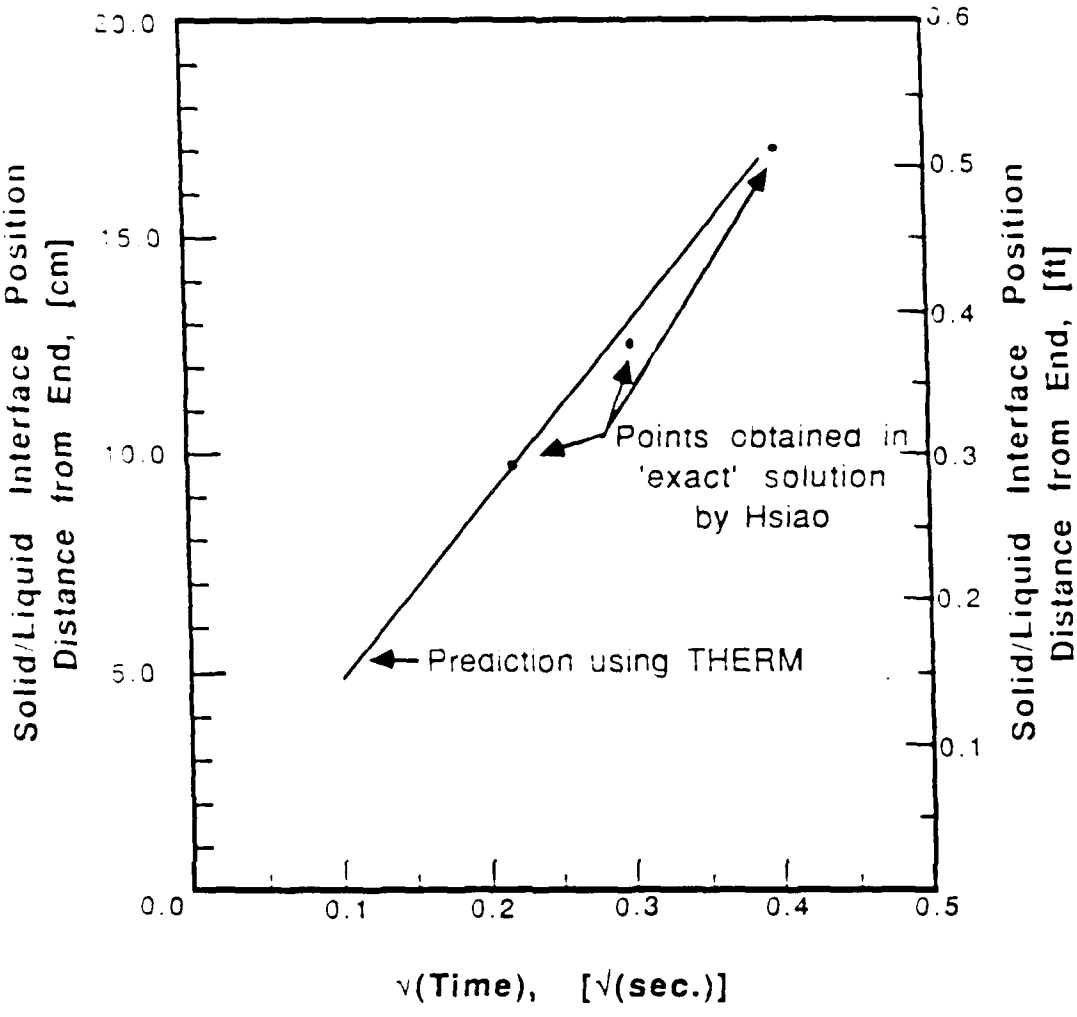

Figure 34. Position of solidification front in the one-dimensional test problem as a function of time. Line represents the prediction obtained using THERM and points represent literature solution [27].

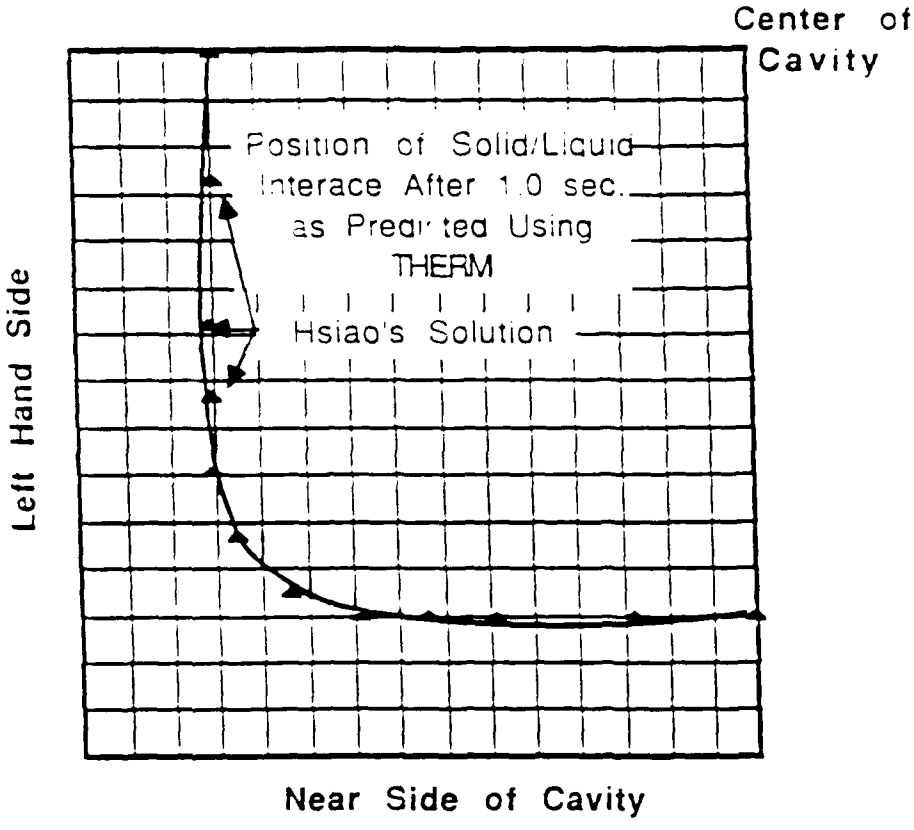

Figure 35. Position of solidification front in the two-dimensional test problem. Line represents the prediction obtained using THERM and points represent literature solution [27].

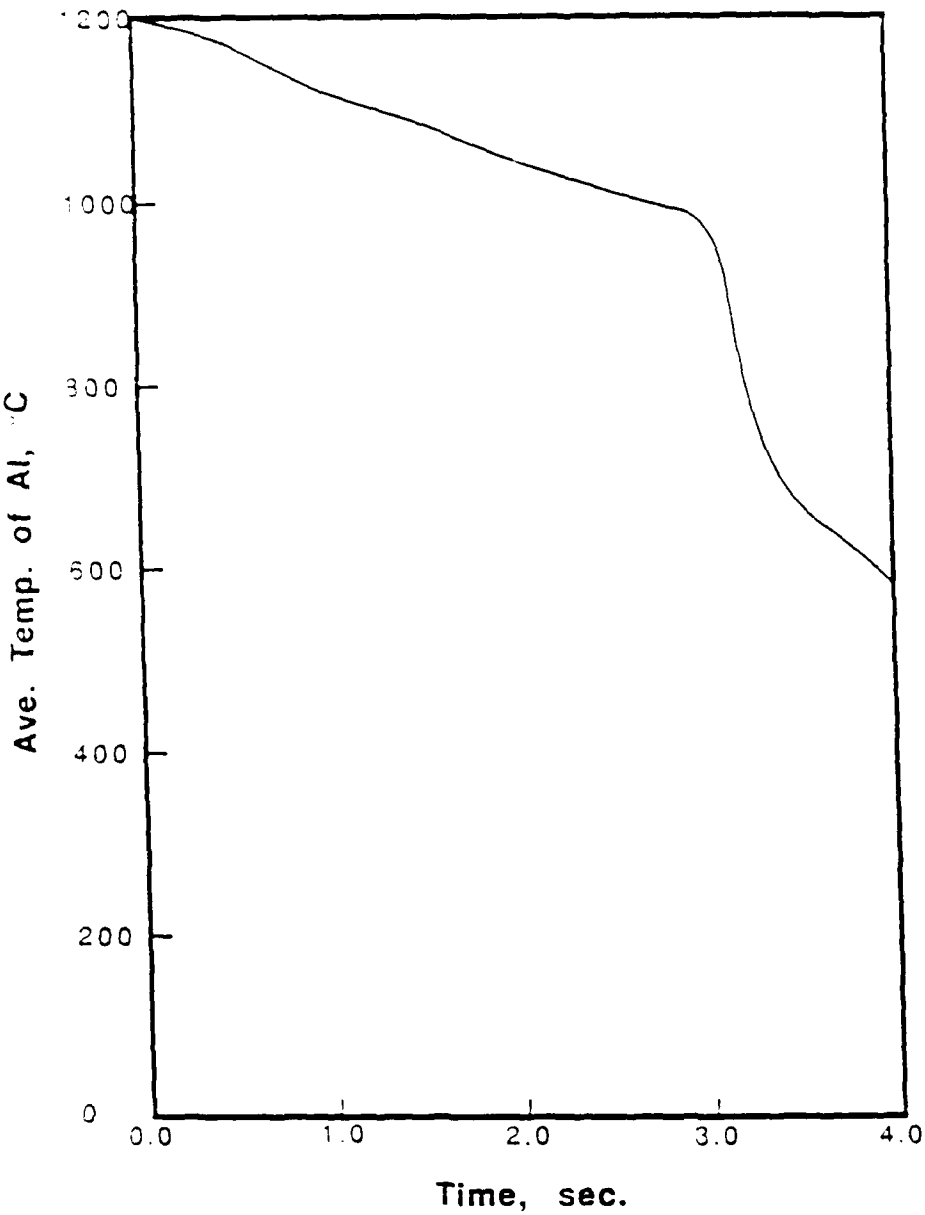

Figure 36. Average temperature of the aluminum alloy as a function of time during the squeeze casting process

the alloy but it still had not reached room temperature. After this time, however, the program began to diverge and was eventually aborted. Further investigation is needed to determine and correct the exact cause of the divergence. Up to the point where the program diverged, however, the results can be considered reliable since they met the convergence criteria specified in the input file.

Chapter 6.

CONCLUSIONS AND RECOMMENDATIONS FOR FUTURE RESEARCH

Unidirectional graphite fiber reinforced aluminum alloy castings have been successfully fabricated using high pressure squeeze casting. Fiber volume fractions for test specimens ranged from 10 to 50 percent. There was a minimum amount of reaction between the graphite fibers and the aluminum matrix in the as-cast condition, good infiltration of the metal into the fiber tows and good fiber distribution. Castings heat treated at very high temperatures showed progressively more reaction. The tensile strength of the as-cast reinforced aluminum increased with increasing fiber volume fraction. Although, in general, the strengths were well below rule of mixtures values. A model, with the assumption that the fiber/matrix interface bond slipped prior to fiber failure, was developed to describe the experimental data. The microhardness of the squeeze cast aluminum was shown to be highest in the as-cast condition (comparable to 6061-T4 Al) and decreased with heat treatment due to overaging. The damping was found to be higher when the fibers were oriented perpendicular to the long dimension of the test beams and relatively constant over the range of fiber volume fractions studied. The transient thermal behavior of the molten aluminum during the squeeze casting process was modelled using finite element methods. The average temperature of the

aluminum reached about 855 K approximately 4 seconds after being introduced to the die at 1473 K.

A review of the results from the experimental work performed leads to several recommendations that may be made for future investigations. A thorough investigation into the effects of heat treatment of the fiber reinforced castings on their physical and mechanical properties needs to be performed. If as expected, the heat treatment increases the strength of the bond between the fibers and the matrix, there may exist an optimum heat treatment beyond which the properties of the castings begin to decline due to degradation of the fibers. Another area requiring further investigation is the refinement of the model developed to describe the thermal behavior of the high pressure squeeze casting process. Such refinement may include the addition of a time variable mesh that will eliminate the requirement for dividing the process into discrete steps as was done in this study.

REFERENCES

1. Plyatskii, V., Extrusion Casting, Primary Sources, New York (1975).

2. Reddy, G. and Murthy, G., "Liquid Forging of an Aluminum Alloy," *Transactions Indian Institute of Metallurgy*, Vol. 31 (1978), pp 484-487.

3. Bhagat, R., Investigation on the Fabrication of Stainless Steel Fiber Reinforced Aluminum Composites, Ph. D. Thesis, Indian Institute of Technology, Bombay, (1981).

4. Nomoto, M., "Mechanical Properties of Squeeze Castings in Al-Cu Alloys," *Journal Japan Institute Light Metals*, Vol. 30 (1980), pp 212-216.

5. Kaneko, Y., Murakami, H., Kuroda, K. and Nagazaki, S., "Squeeze Casting of Aluminum," *Foundry Trade Journal*, Vol. 148 (1980), pp 397-411.

6. Ishimaru, H., Kaneko, J. and Sugamata, M., "Effect of High Pressure Casting on Properties of Aluminum Casting Alloys," *Journal Japan Institute of Light Metals*, Vol. 31 (1981), pp 712-719.

7. Suzuki, S., "Segregation of Aluminum Alloys Solidified under High Pressure," *Journal Japan Institute Light Metals*, Vol. 32 (1982), pp 395-401.

8. Chatterjee, S. and Das, A., "Some Observations on the Effect of Pressure on the Solidification of Al-Si Eutectic Alloys," *British Foundryman*, Vol. 66 (1973), pp 118-124.

9. Williams, G. and Fisher, K., "Squeeze Forming of Aluminum Components," *Metals Technology*, Vol. 8 (1981), pp 263-267.

10. Franklin, J. and Das, A., "Squeeze Casting--Review of the Status," *British Foundryman*, Vol. 77 (1984), pp 150-158.

11. Allison, C., Effect of Pressure on the Solidification of Aluminum-Silicon Alloys, Ph. D. Dissertation, University of Cincinnati, Cincinnati, OH, (1969).

12. Benedyk, J. and Shaw, W., "Squeeze Casting of Aluminum--New Metal Working Process," *Light Metal Age*, Vol. 27 (1969), pp 6-8.

13. Kulkarni, K., "Squeeze Casting Comes of Age," *Foundry Management Technology*, Vol. 102 (1974), pp 76-79.

14. Lynch, R., "Squeeze Casting of Aluminum," *AFS Transactions*, Vol. 83 (1975), pp 569-576.

15. Nisida, Y. and Matsubaru, H., "Effect of Pressure on Heat Transfer at the Metal-Mould Interface," *British Foundryman*, Vol. 69, No, 11 (1976), pp 276-278.

16. Sandler, S., Chemical and Engineering Thermodynamics, Wiley, New York, NY (1977), pp 250-252.

17. Delamotte, E., Phillips, K., Perry, A. and Kilas, H., "Continuously Cast Aluminum-Carbon Fiber Composites and Their Tensile Properties," *Journal of Materials Science*, Vol. 7 (1972), pp 346-349.

18. Amateau, M., "Progress in the Development of Graphite-Aluminum Composites using Liquid Infiltration Technology," *Journal of Composite Materials*, Oct. (1976), pp 279-295.

19. Girot, F., Fedou, R., Quenissot, J. and Naslain, R., "On the Squeeze casting Conditions of Aluminum Matrix Composite Materials," *American Society for Composites, Second Annual Conference Proceedings*, Sept. 1987, pp 361-370.

20. Kohara, S. and Muto, N., "Degradation of Carbon Fibers in Molten Aluminum," *Developments in Science and Technology of Composite Materials, ECCM Conference Proceedings*, (1985), pp 738-743.

21. Bhagat, R. and Amateau, M., "High Pressure Casting of Metal Matrix Composites," Presented during Materials Week '87, Cincinnati, OH, Oct. 1987.

22. Bhagat, R., "High Pressure Squeeze Casting of Stainless Steel Wire Reinforced Aluminum Matrix Composites," Accepted for publication in *Composites* to appear in Sept. 1988.

23. ASM Metals Handbook, Ninth Edition, Vol. 3, Properties and Selection: Non-Ferrous Alloys and Pure Metals, ASM, Metals Park, OH, (1979), pp 45, 54 and 61.

24. Agarwal, B. and Broutman, L., Analysis and Performance of Fiber Composites, Wiley, New York, NY (1980), p. 80.

25. Bathe, K., Finite Element Procedures in Engineering Analysis, Prentice Hall, Englewood Cliffs, NJ (1982), pp 407-428, 339, 490 and 554.

26. Sonti, N., Influence of Process Parameters on Laser Weld Characteristics in Aluminum Alloys, Ph. D. Thesis, Pennsylvania State University, University Park, PA, (1988), pp 46-52.

27. Hsiao, J., "An Efficient Algorithm for Finite Difference Analysis of Heat Transfer with Melting and Solidification." *Numerical Heat Transfer*, Vol. 8 (1985), pp 653-666.

28. Bhagat, R., Amateau, M., Conway, J., Paulick, J., Chisholm, J., Parnell, J. and Seidensticker, D., "Squeeze Cast Metal Matrix Composites: Evaluation of Their Strength, Damping capacity and Corrosion Resistance." Submitted to *Journal of Composite Materials*, (1988)

29. Reed-Hill, R. F., Physical Metallurgy Principles, 2nd ed., Van Nostraud, (1973).